

**Acoustic Scattering of Broadband Echolocation
Signals from Prey of Blainville's Beaked Whales:
Modeling and Analysis**

by

Benjamin A. Jones

B.S., United States Naval Academy, 1997

Submitted in partial fulfillment of the requirements of the degree of

Master of Science

at the

MASSACHUSETTS INSTITUTE OF TECHNOLOGY

and the

WOODS HOLE OCEANOGRAPHIC INSTITUTION

September 2006

© Benjamin A. Jones, 2006. All rights reserved.

The author hereby grants to MIT and WHOI permission to reproduce and distribute publicly paper and electronic copies of this thesis document in whole or in part.

Author
Joint Program in Oceanography/Applied Ocean Science and Engineering
September 2006

Certified by
Andone C. Lavery, Assistant Scientist
Thesis Co-Supervisor

Certified by
Timothy K. Stanton, Senior Scientist
Thesis Co-Supervisor

Accepted by
Henrik Schmidt, Professor of Mechanical Engineering
Chair, Joint Committee for Applied Ocean Science and Engineering

Accepted by
Lallit Anand, Professor of Mechanical Engineering
Chairman, Graduate Committee

Acoustic Scattering of Broadband Echolocation Signals from Prey of Blainville's Beaked Whales: Modeling and Analysis

by

Benjamin A. Jones

Submitted in partial fulfillment of the requirements for the degree of
Master of Science

at the Massachusetts Institute of Technology
and the Woods Hole Oceanographic Institution

Abstract

Blainville's beaked whales (*Mesoplodon densirostris*) use broadband, ultrasonic echolocation signals (27 to 57 kHz) to search for, localize, and approach prey that generally consist of mid-water and deep-water fishes and squid. Although it is well known that the spectral characteristics of broadband echoes from marine organisms are a strong function of size, shape, orientation and anatomical group, little is known as to whether or not these or other toothed whales use spectral cues in discriminating between prey and non-prey. In order to study the prey-classification process, a stereo acoustic tag was mounted on a Blainville's beaked whale so that emitted clicks and corresponding echoes from prey could be recorded. A comparison of echoes from prey selected by the whale and those from randomly chosen scatterers suggests that the whale may have, indeed, discriminated between echoes using spectral features and target strengths. Specifically, the whale appears to have favored prey with one or more deep nulls in the echo spectra as well as ones with higher target strength.

A three-dimensional, acoustic scattering model is also developed to simulate broadband scattering from squid, a likely prey of the beaked whale. This model applies the distorted wave Born approximation (DWBA) to a weakly-scattering, inhomogeneous body using a combined ray trace and volume integration approach. Scatterer features are represented with volume elements that are small (less than $1/12^{th}$ of the wavelength) for the frequency range of interest (0 to 120 kHz). Ranges of validity with respect to material properties and numerical considerations are explored using benchmark computations with simpler geometries such as fluid-filled spherical and cylindrical fluid shells. Modeling predictions are compared with published data from live, freely swimming squid. These results, as well as previously published studies, are used in the analysis of the echo spectra of the whale's ensonified targets.

Thesis Co-Supervisor: Andone C. Lavery
Title: Assistant Scientist

Thesis Co-Supervisor: Timothy K. Stanton
Title: Senior Scientist

Acknowledgments

Nearly a decade ago as I began working in Naval aviation, I could not have imagined the wonderfully crooked path which my career would follow. The opportunity to take a two year hiatus from operational duties to pursue scientific research has fulfilled a dream. Without the advocacy of my entire chain of command, particularly CDR Michael “Reggie” Hammond and CAPT Tom Webber, and the financial support from the Office of the Oceanographer of the Navy the work here could not have been conducted.

I cannot fully express my appreciation for the support that I have received from my research advisors at the Woods Hole Oceanographic Institution. Dr. Tim Stanton, who swept me into his realm of acoustic scattering on my first day at WHOI, has a gift of enthusiasm for his work which he will bequeath on anyone fortunate enough to become involved. Dr. Andone Lavery has had the unenviable job of turning a seven year Naval officer into a nascent acoustician. I am truly grateful for her unwavering support, tireless tutoring, and always elegant way of approaching difficult problems.

The unique environment at WHOI, where barriers between research departments seem to blow away in the salty breeze, has been key to this research. My coauthors for the article on which Ch. 2 is based, biologists Dr. Peter Tyack and Dr. Peter Madsen and electrical engineer Dr. Mark Johnson, introduced me to the fascinating world of deep-diving, echolocating whales where sound illuminates the darkness. The data from the tagging of a Blainville’s Beaked whale, collected with support from National Oceanographic Partnership Program, the Office of Naval Research, and Canary Islands Government, was graciously provided by them.

The modeling section of this study could not have been completed without the energetic support of Dr. Darlene Ketten and her talented staff of technical experts, particularly Julie Arruda, R.T.(R) who conducted the CT scans of squid presented here and Sr. Research Asst. Scott Cramer who aided in the handling, transport, and preservation of the specimens. The excellent squid specimens used in this study were identified and provided by Ed Enos, Superintendent of the Aquatic Resources

Division at Marine Biological Laboratory. I would also like to mention Dr. Roger Hanlon with whom, on more than one occasion, enlightening discussions were held on the natural history of squid.

Finally, I would like to thank my spouse, Sylvie Rusay, whose endless wit and wisdom have protected my sanity through many long and often difficult academic and research hurdles. Thank you, my dear.

Contents

1	Introduction	15
1.1	Historical background on echolocation research	15
1.1.1	Echolocation in bats	15
1.1.2	Echolocation in toothed whales	16
1.2	Broadband scattering from marine organisms	18
1.3	Modeling of broadband acoustic scattering	19
1.4	Overview of study	21
2	Classification of broadband echoes from prey of a foraging Blainville’s beaked whale	23
2.1	Introduction	23
2.2	Signals emitted by the Blainville’s beaked whale (<i>M. densirostris</i>) . .	24
2.2.1	FM clicks	25
2.2.2	Buzz clicks	26
2.3	Acoustic data acquisition	26
2.3.1	Instrumentation (Digital Acoustic Recording Device, DTAG) .	26
2.3.2	Fieldwork	27
2.4	Data analysis	29
2.4.1	Selection criteria of echoes	29
2.4.2	Spectral classification	32
2.4.3	Target strength calculations	33
2.5	Results	36
2.5.1	Echoes selected for analysis	36

2.5.2	Echo classification	36
2.5.3	Comparison of echo characteristics between two groups of prey	41
2.5.4	Comparison between echo characteristics and scattering predic- tions/observations	43
2.6	Discussion	45
3	Acoustic scattering by weakly scattering shelled objects: Applica- tion to Squid	47
3.1	Introduction	47
3.2	Theory	49
3.2.1	Basic definitions	49
3.2.2	DWBA-based scattering models	51
3.2.3	Exact modal-series-based scattering models	53
3.3	Materials and methods	54
3.3.1	Animals studied	54
3.3.2	High resolution morphometry of squid: SCT scans	57
3.3.3	Numerical implementation of the DWBA ray-tracing model	58
3.3.4	Application to squid	60
3.4	Results	61
3.4.1	Scattering from fluid-filled, fluid spherical and finite cylindrical shells	61
3.4.2	Application to squid	68
3.5	Discussion	71
4	Summary and conclusion	75
4.1	Scattering of echolocation signals	75
4.2	Modeling	76
4.3	Recommendations for future work	76
4.4	Contributions of this thesis	77

A	Modal series coefficients for fluid-filled shells	79
A.0.1	Spherical shells	79
A.0.2	Cylindrical shells	80
B	Algorithms for DWBA ray-tracing model	81

List of Figures

2-1	Echolocation signal (FM click) of the <i>M. densirostris</i>	25
2-2	Echograms of scattered echolocation signals of a foraging beaked whale	28
2-3	Example of automated structure analysis.	32
2-4	Broadband acoustic signatures of four prey selected by the whale. . .	35
2-5	Characteristics of echo trains “selected” by the whale, and randomly chosen “non-selected” scatterers.	37
2-6	Depth distribution of two groups of prey categorized by echo density.	41
2-7	Spectral content in frequency responses of “selected” prey and “non- selected” scatterers.	42
2-8	Reduced target strength distribution of prey “selected” by the whale and “non-selected” scatterers.	44
3-1	Diagram of the bisection of spherical shell or cross section of a cylin- drical shell illustrating inhomogeneous material properties.	50
3-2	Sketches of two squid species, <i>L. pealeii</i> and <i>T. pacificus</i>	55
3-3	Volume rendering composed of SCT images of squid and four binary cross sections.	56
3-4	Ray trace illustration through inhomogeneous volume.	58
3-5	Effect of varying shell thickness on reduced target strength for a spher- ical, fluid-filled, fluid shell.	62
3-6	Effect of varying shell thickness on reduced target strength for a cylin- drical, fluid-filled, fluid shell of finite length.	64

3-7	Effect of varying material properties on reduced target strength for a cylindrical, fluid-filled, fluid shell of finite length.	65
3-8	Reduced target strength versus orientation predictions for solid cylinder of finite length.	67
3-9	Reduced target strength predictions for various tilt angles of squid compared with published data of freely swimming and anesthetized squid.	69
3-10	Average reduced target strength predictions of squid	70

List of Tables

2.1	Distribution of echoes from “whale-selected” and “non-whale-selected” echo trains in the three dives examined.	38
3.1	Material properties of squid from published sources.	57

Chapter 1

Introduction

1.1 Historical background on echolocation research

Echolocation is a term coined by Griffin (1944) for an animal's emission of high frequency sounds and the consequent reception of echoes for use in obstacle avoidance. This ability, also now known to be used in hunting for prey, has been most thoroughly documented in two very distinct taxa of mammals. Most species of the suborder *Odontoceti*, or toothed whales, use echolocation including members of the family *Ziphiidae*, or beaked whales (Johnson *et al.*, 2004; Madsen *et al.*, 2005; Zimmer *et al.*, 2005). Likewise, sound is used by the small flight-capable mammals, *Chiroptera*, or bats. Both of these groups of mammals have evolved echolocation capabilities for use in the absence of light. While bats use sound to navigate and hunt on the wing at night, beaked whales use echolocation to hunt for prey at ocean depths where significant sunlight cannot penetrate. A brief review of research on these animals' biosonar, summarized in the following paragraphs, provides context for this study.

1.1.1 Echolocation in bats

Researchers have debated for over two centuries the capabilities of certain species of animals to use biosonar in orientation, communication, and prey capture. As early as 1793 Italian scientist Lazzaro Spallanzani and Swiss zoologist Louis Jurine discovered

that bats depend primarily on hearing rather than sight for orientation in dark environments (Galambos, 1942). Spallanzani conducted extensive experiments in which blinded bats avoided slender obstacles, such as silk threads suspended from the ceiling, with the same success as visually unhindered bats. After repeating Spallanzani's experiments on blinded bats, Jurine provided conclusive evidence that bats rely heavily on hearing to navigate. In a series of experiments in which bats' ears were plugged with a variety of substances, such as wax and wood, the animals crashed aimlessly into obstacles in their path.

It was not until much later, however, with the development of G.W. Pierce's ultrasonic detector, that Pierce and Griffin (1938) collected data to support theories that bats use ultrasonic emissions to provide spatial orientation. Evidence of hunting minute insects using active sonar would not be found for another decade and a half (Griffin, 1953). This, in turn, has led researchers to question the extent to which bats can acoustically resolve their environment. Simmons and Vernon (1971) showed that the big brown bat (*Eptesicus fuscus*), using broadband frequency modulated (FM) clicks, can indeed discriminate size, shape, and distance to targets. Furthermore, Siemers and Schnitzler (2000) have shown that the Natterer's bat (*Myotis nattereri*), also using FM signals, can discriminate prey from background clutter using echolocation without the aid of passive secondary cues such as prey-generated sounds or olfactory information. Bats' use of frequency dependent cues found in echoes from objects that they ensonify is an area of ongoing research (Simmons and Chen, 1989; Schmidt, 1992; von Helversen and von Helversen, 2003). Recently, it has been suggested that bats use spectral information from sequences of target echoes to discriminate between differing shapes and sizes (von Helversen, 2004). This line of research, which gives strong evidence that bats do make use of spectral cues in object discrimination, provides motivation to explore similar adaptations in toothed whales.

1.1.2 Echolocation in toothed whales

Historically, studies on echolocation capabilities of the sub-order *Odontoceti*, toothed whales, have concentrated on various species of dolphins in captivity. It is well-known

that these animals transmit a variety of broadband, ultrasonic signals in order to navigate and hunt their prey. Many tank experiments, using artificial targets with subtle differences in size, shape and material compositions, have shown that dolphins use information contained in the broadband echoes to aid in discrimination tasks (Nachtigall, 1980). Identifying the features of acoustic signals that dolphins use in these tasks is a goal of ongoing research. Au and Pawloski (1989) have shown that dolphins can discriminate between broadband signals having a “rippled” or “non-rippled” frequency spectra. Fuzessery *et al.* (2004), cites experiments by Vel’min and Dubrovskiy (1976), and Dubrovskiy (1989), where dolphins discriminate between pulse pairs with intervals of 0.05 to 0.2 ms, much shorter than the dolphin’s auditory integration time of 0.3 ms given by Au (1993). It is suggested that dolphins, which would perceive these pulse pairs as a single echo, may be processing them in the frequency domain. With respect to the inverse problem, research on acoustic scattering from marine organisms has shown that different groups of animals can be classified by the frequency spectra of their backscattered signal (Martin *et al.*, 1996; Stanton *et al.*, 1998b). It is unclear, however, to what degree dolphins, or other toothed whales, use features of broadband, acoustic backscattering to aid in the classification of prey.

The limited number of *in situ* studies on echolocating toothed whales has limited progress in this area of research. In many species the combination of depth of the echolocating animal and attenuation of the high frequency signal prevent either ship mounted or towed sensors from recording their emitted signals. A number of recent studies, using new technologies and novel methods, have begun to advance the understanding of these animals’ behavior in their natural environment. Using hydrophone arrays deployed from small boats to record whales foraging by echolocation (Au *et al.*, 2004) and newly developed acoustic data tags affixed directly to echolocating whales (Johnson and Tyack, 2003; Akamatsu *et al.*, 2005; Zimmer *et al.*, 2005; Madsen *et al.*, 2005) researchers have started to collect new information about the echolocation signals and foraging behavior of free-ranging toothed whales. The analysis presented in Ch. 2 of this thesis is based upon data collected from such a study in which an acoustic tag recorded a beaked whale echolocating in the wild.

1.2 Broadband scattering from marine organisms

In complement to the research on the biosonar systems of these capable predators, a concurrent body of research has been conducted on acoustic scattering from marine organisms of lower trophic levels. Attempts to estimate zooplankton biomass have highlighted the need for accurate acoustic characterization of various classes of zooplankton (Stanton *et al.*, 1994; Martin *et al.*, 1996). Constructive and destructive interference of the sound wave scattered by features such as tissue interfaces or skeleton create a frequency dependent interference pattern specific to orientation, material properties (i.e. sound speed and density), and morphology of the scatterer. Models that predict frequency specific scattering amplitude from different organisms can aid in the remote classification and identification of species being surveyed.

Recent trends in fisheries research have followed a similar course. Through the use of multibeam sonars, multiple discrete frequencies, and higher bandwidth systems, researchers have improved spatial resolution of fish schools and species identification during acoustic surveys (Horne, 2000). Broadband acoustic systems have been used with a variety of processing techniques in efforts to conduct reliable species recognition based on the spectral signature of backscatter from fish aggregations (Simmonds *et al.*, 1996; Zakharia *et al.*, 1996). Broadband scattering from individual, swimbladder-bearing fish has also been investigated. Reeder *et al.* (2004) has shown that high frequency acoustic backscatter from alewife is highly frequency dependent as well as strongly affected by orientation. Combining this insightful research on scattering from marine organisms with the knowledge that echolocating whales use broadband, ultrasonic biosonars leads to the hypothesis that an acoustic basis for prey discrimination exists in the frequency dependent characteristics of the prey echoes. It is the goal of this study to elucidate specific characteristics found in prey echoes of a free-ranging beaked whale that may be used by the whale to discriminate between prey and non-prey scatterers in the water column.

1.3 Modeling of broadband acoustic scattering

Modeling of acoustic scattering from individual marine organisms complements laboratory and field measurements by helping to quantify factors that influence the scattering of sound. Furthermore, extracting biologically important information, such as species type and abundance, from high-frequency, acoustic scattering data relies heavily on the availability of experimentally validated scattering models (see review by Horne (2000)). The intended application of a model often dictates the level of complexity used in representing a marine organism as a scatterer. These applications range from predictions of volume scattering, which may use discrete scattering predictions averaged over a range of parameters such as size and orientation of the scatterer, to models that attempt to replicate discrete echoes for unique identification of class, size, or even species of scattering organism.

In general acoustic scattering from individual marine organisms is a complex process that is dependent on the frequency of the incident sound wave, the orientation of the scatterer with respect to the incident wave, and the size, morphology, and material properties (i.e. density and sound speed) of the organism. Scattering by organisms of widely varied anatomical groups have been modeled. Fish, both swimbladder-bearing and non-swimbladder-bearing, have been extensively modeled for use with acoustic survey data to estimate fish stocks (see reviews by Maclennan and Simmonds (1992); Foote (1997)). Zooplankton models have, likewise, been developed for use with echo sounder surveys. The diversity of organisms within zooplankton populations is reflected in the variety of models developed (see review by Foote and Stanton (2000)).

One group of zooplankton that researchers have focused on are weakly-scattering organisms with fluid-like material properties (i.e. tissue that does not support shear waves). Many advances have been made in developing high frequency acoustic scattering models for this group of organisms involving shapes of varying complexity. The representation of shape in early studies were based on fluid models of simple geometric volumes such as spheres, finite cylinders, and prolate spheroids (Anderson,

1950; Yeh, 1967; Johnson, 1977; Stanton, 1988). More recent models have incorporated high resolution 2-D (Stanton *et al.*, 1998a; McGehee *et al.*, 1998; Amakasu and Furusawa, 2006) and 3-D (Lavery *et al.*, 2002) details of zooplankton shape. The complex representation of shape in these models are made possible by the application of the distorted wave Born approximation (DWBA). This modification to the Born approximation (BA), a volume integral formulation for weakly scattering bodies, can account for complex 3-D shape as well as inhomogeneous material properties. The DWBA formulation has been successfully applied to model the scattering of sound from various types of zooplankton including euphausiids, copepods, krill and decapod shrimp and validated through field measurements (Wiebe *et al.*, 1997; Lawson *et al.*, 2004).

Incorporation of high resolution material properties into DWBA models such that variations correspond to the anatomical structure of the organism being simulated is still a challenge. Limited information on sound speed and density of different tissues within marine organisms, as well as difficulties in implementing the DWBA for inhomogeneous bodies, are the primary obstacles. Application of the DWBA has been primarily limited to scattering bodies of homogeneous material properties (Stanton *et al.*, 1993; Chu *et al.*, 1993; Stanton *et al.*, 1998a; McGehee *et al.*, 1998; Stanton and Chu, 2000; Lavery *et al.*, 2002). Yet, marine organisms have complex internal morphologies, which include internal organs (e.g. lungs, liver, gonads, etc.), and may also include large seawater filled cavities as found in squid or jellyfish. These internal structures of differing material properties create multiple interfaces that strongly affect the scattering of sound. The DWBA has been applied to inhomogeneous volumes by varying material properties along the length of an organism's body (Stanton *et al.*, 1998a; Stanton and Chu, 2000; Lavery *et al.*, 2002). In these cases variation corresponded to general body composition such as segmentation of the exoskeleton. To date, however, 3-D inhomogeneities due to internal structure of an organism's body have not been incorporated into a DWBA model. The modeling section of this thesis presents a DWBA model that can accurately account for 3-D inhomogeneities within a weakly-scattering body. This model is applied to squid, a common prey of

beaked whales, using high resolution morphology obtained from spiral computerized tomography (SCT) scans. Results from this modeling is used in the analysis of beaked whale prey discussed in Ch. 1.

1.4 Overview of study

This thesis is organized as follows. Chapter 2 presents an analysis of broadband echoes, recorded *in-situ*, from prey of an echolocating beaked whale. Chapter 3 reports on the development of an advanced model for weakly scattering bodies that incorporates both detailed, 3-D shape and 3-D material property inhomogeneities of the scatterer. Chapter 4 contains concluding remarks and contributions of this paper to the scientific community. Coefficients of the modal-series-based solutions for fluid shells and the algorithms used in the numerical scattering model are given in the appendices.

Chapter 2

Classification of broadband echoes from prey of a foraging Blainville's beaked whale ¹

2.1 Introduction

In a recent study non-invasive digital acoustic recording devices, DTAGs (Johnson and Tyack, 2003), were attached to a Blainville's beaked whale, (*Mesoplodon densirostris*) and used to record echolocation signals during deep foraging dives (Johnson *et al.*, 2004). These whales use broadband signals to search for and localize prey consisting of mesopelagic fishes and squid (Pauly *et al.*, 1998). Acoustic data recorded by the DTAG contained both the whale's emitted signals as well as echoes from prey in the water column. These data show that, although the whale ensonified a large number of scatterers, it only actively pursued a small percentage of them. This suggests that the animal is actively selecting certain types of prey (Madsen *et al.*, 2005). In this paper, these data are examined to determine if there is evidence of an acoustic basis for target discrimination based on the scattering of their echolocation signals. Singly resolvable echoes from prey selected by the whale and from non-

¹This chapter is based on an article to be submitted to the Journal of the Acoustical Society of America (Jones *et al.*, in prep.b)

selected scatterers in the water column are compared using spectral characteristics and relative target strengths. Secondly, two populations of depth separated prey are juxtaposed to provide a comparison of two, likely different prey types. Finally, the results are discussed in context with experimental and modeling results of scattering from marine organisms.

Conducting an analysis of echoes, recorded *in situ*, using the whale's biosonar as a sound source and the animal's body as the platform for the receiver present a myriad of difficulties. These challenges and how they are addressed, which are discussed in detail in the following sections, are summarized: 1) It was not feasible to make far field measurements of the sounds emitted by the whale. Instead, as a reference for the frequency responses of the scatterers, the featureless portion of the frequency spectrum of an echolocation signal recorded from another whale of the same species is used. 2) The near-field recording of the whale's emitted signal is used as a proxy for changes in the amplitude of the emitted signal. Thus, relative target strengths of the scatterers can be obtained. 3) The unpredictability of the platform, i.e. the whale, has a significant effect on the position of the scatterer within the beam. The angle of arrival information from the hydrophone pair is used to limit, in one dimension, the position of the scatterer with respect to the longitudinal centerline of the whale. Using this carefully constrained subset of the data, it is demonstrated that there are significant differences with respect to relative target strengths and spectral content between echoes of prey selected by the whale and non-selected scatterers.

2.2 Signals emitted by the Blainville's beaked whale (*M. densirostris*)

The *M. densirostris* transmits two distinct echolocation signals. Johnson et al., (submitted) discriminates between these signals based on their repetition rate, waveform, and frequency content. A slow repetition rate signal (referred to here as FM clicks) is used by the whale in the search and approach of prey while a high repetition rate

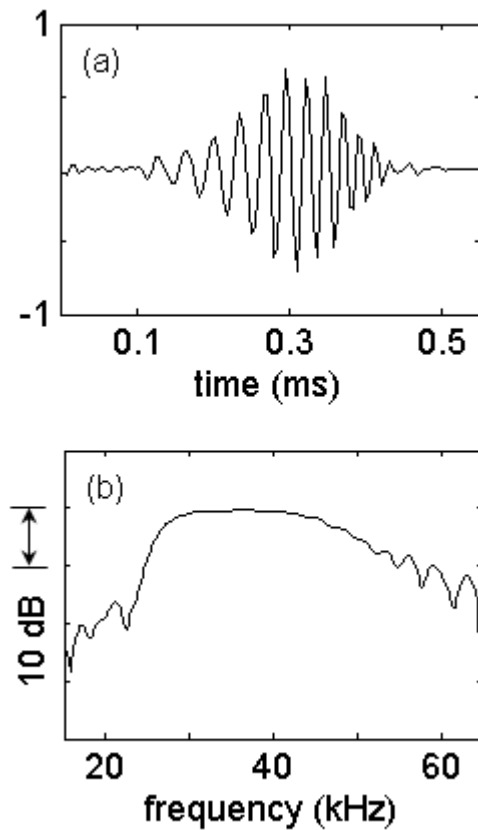


Figure 2-1: Echolocation signal (FM click) of *M. Densirostris*: (a) normalized time series, (b) frequency spectrum.

signal, called buzz clicks, is used during the terminal portion of a prey capture.

2.2.1 FM clicks

The FM clicks, following the nomenclature of Johnson *et al.* (submitted), are characterized by an upswept, frequency modulated waveform of 220 to 320 μ s in length. They are produced nearly continuously at depth while the animal is searching for and localizing prey. The inter-click-interval (ICI) for the FM clicks ranges from 0.1 to 0.6 s. The associated frequency spectrum is smoothly shaped between approximately 25 to 54 kHz with a rapid fall off at lower frequencies and has -10 dB endpoints at 27 and 57 kHz (Fig. 2-1). It has been shown by Johnson *et al.* (submitted) that the

frequency content of these clicks, when recorded on axis, is generally consistent from ping to ping. Throughout this analysis only echoes from targets ensonified by FM clicks are considered.

2.2.2 Buzz clicks

When approaching prey to within approximately a body length, the *M. densirostris* switches to a high-repetition-rate click. These clicks are approximately half the duration of the FM clicks and are of significantly lower amplitude. This series of clicks, referred to collectively as a *buzz*, is often accompanied by a rapid acceleration of the whale and is believed to be associated with the final homing and capture phase of the hunt (Johnson *et al.*, 2004). Buzzes are used in this analysis to identify the whale's selected prey.

2.3 Acoustic data acquisition

A free-ranging beaked whale was tagged with a digital acoustic recording device, DTAG. The tag was used to record echolocation signals emitted by the whale as well as echoes from scatterers in the water column. It is the characteristics of the echoes from scatterers in the water column that are of particular interest to this study.

2.3.1 Instrumentation (Digital Acoustic Recording Device, DTAG)

The DTAG is a small, self-contained device designed to record acoustic and orientation data from a freely swimming animal (Johnson and Tyack, 2003). This tag attaches to the surface of a whale with four suction cups, which actively release after a pre-set period of time. The version used to collect the data presented in this paper contains two hydrophones spaced 2.5 cm apart, each with a frequency response that is constant to within 3 dB between 0.4 and 67 kHz and with a sensitivity of -171 dB re $V/\mu Pa$ in that band. The tag samples acoustic data from each of the hydrophone channels at

a rate of 192 kHz. Also included in the tag’s sensor suite were 3-axis accelerometers and 3-axis magnetometers for orientation and a pressure sensor for extracting depth. These sensors record data at a 50 Hz sampling rate. Data are stored in a non-volatile FLASH memory array with a capacity of 6.6 gigabytes.

2.3.2 Fieldwork

An adult, female Blainville’s beaked whale (MD287a) was tagged in October of 2004, near the island of El Hierro, in the Canary Islands, by means of a 5-meter-long carbon fiber pole from a 4-meter-long rigid-hull inflatable boat (RHIB). The animal was observed surfacing from a 7-meter-long RHIB during daylight hours, which included the acoustic portion of the recording. The tag recorded acoustic data for the preprogrammed time of 9.5 hours. A reserve of memory allowed the logging of an additional 8.9 hours of orientation and depth data after which the tag automatically released. The tag was located and recovered with the aid of a VHF transmitter included in the tag.

The tag was initially placed on the right side of the whale, but moved to a position approximately 1 meter posterior of the blowhole on the animal’s dorsal ridge prior to the dives discussed in this paper. This position, fortuitously, minimized shading of the hydrophones by the whale’s body and provided favorable conditions for recording echoes from objects ensonified by the whale. One intrinsic difficulty with a tag located behind a whale’s head, is that only near-field, off-axis transmissions can be recorded (Johnson *et al.*, 2004). These measurements, clearly, do not reflect actual source levels within the animal’s forward beam. However, measurements of transmitted signals from a tag in this position can provide a proxy for relative changes in the power output of the whale’s clicks (Madsen *et al.*, 2005). Thus, it is possible to estimate ping-to-ping variation in source level.

Three dives are discussed in this paper, dives #2 - #4. During these dives FM clicks were only recorded at depths greater than 440m while the whale dove to various depths down to 1300 m. During dive #3 the whale hunted near the bottom in a narrow band of depth between 600 and 650 m as indicated by the buzzes at these depths.

Foraging during dives #2 and #4 appeared to be spread out in depth over several hundred meters; although, in both cases the majority of buzzes were concentrated in depth bands of less than 200 meters.

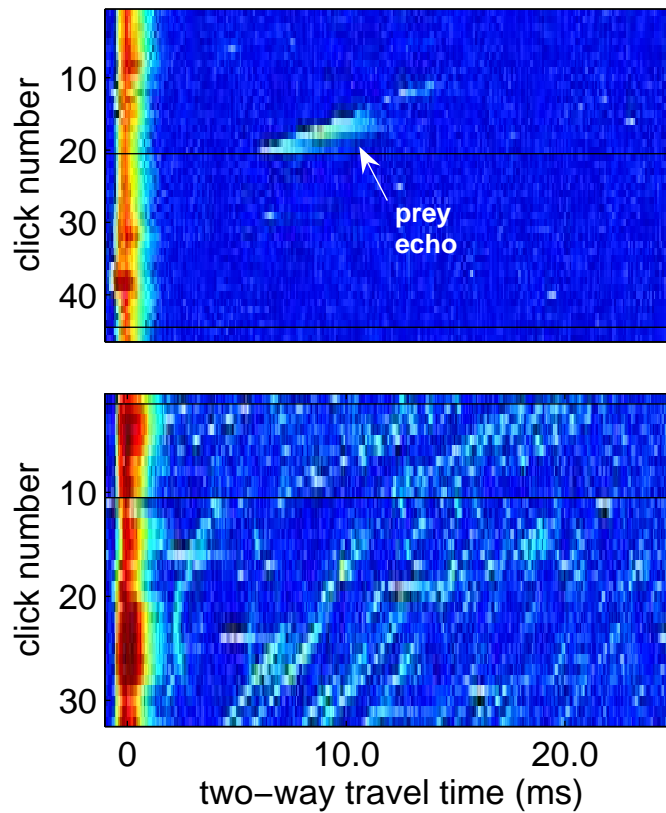


Figure 2-2: Two representative examples of echograms displaying scattered echolocation signals of a foraging beaked whale which are used to identify echo trains: (a) low echo density environment, (b) high echo density environment. FM click number is shown on the y-axis and the x-axis shows time since last emitted click. Echo strength is indicated by color with red corresponding to higher sound pressure and blue corresponding to lower sound pressure. The top plot shows a single echo train as the whale approaches a target. The black line represents a spacing of greater than 1 second between outgoing clicks that meet a pre-set threshold level which, in this case, indicates the whale's switch to the lower amplitude buzz.

2.4 Data analysis

2.4.1 Selection criteria of echoes

Identifying echo trains from whale-selected prey

The acoustic data recorded by the DTAG corresponded to four full dives of this whale. Both the tagged animal's emitted signals and scattered echoes were recorded on all four dives; however, only data from dives #2 through #4 were considered due to the preferred placement of the tag on these dives. Approximately 1.4 hours of acoustic data from these three dives were analyzed.

The acoustic record was analyzed to identify all buzzes, or suspected predation events, that occurred during the three dives of interest. Firstly, an algorithm indicating relative amplitude and time between clicks was used in combination with a time-frequency spectrogram of the signals to identify buzzes. Secondly, echograms were produced indicating sound power on a color scale in a plot of click number versus time (see Fig. 2-2). By aligning the envelopes of the tagged whale's transmitted clicks on one axis and two-way travel time (TWT) along the other, these echograms were used to identify echo trains, or continuous series of echoes from a single scatterer. A 25 ms TWT window was used corresponding to a range from source to scatterer of about 18 m. Using this method prey echo trains were easily identifiable by their slowly varying, and generally, monotonically decreasing TWT.

The echograms were analyzed in the vicinity of the buzzes to identify echo trains from intended prey. Only echo trains associated with regular clicks that terminated within five seconds of a buzz were selected. If multiple echo trains were identified (i.e. series of echoes with different TWT from the same outgoing transmission and, thus, different ranges from whale to scatterer) the echo train that terminated most closely to the first buzz click echo, in time, was selected. If no echo was visible from the buzz in such a case, or two echo trains were very close together in time, that sequence was not considered in the analysis. An identifiable echo from the buzz, however, was not a criterion if there was no ambiguity in selecting the echo train.

Identifying echo trains from non-selected scatterers

Randomly chosen echo trains, not selected by the whale as prey, were identified for processing on each dive. These non-selected echo trains were defined as those that did not immediately precede a buzz from the whale. The same two way travel time window of 25 ms was used to choose these non-selected echo trains.

Acoustic environment: aggregations of varying density

In addition to the discrete echoes, which were selected from the acoustic record, several other parameters were extracted from the data record such as depth and echo density. Each of these data was recorded for the time corresponding to the beginning of the identified echo train. Echo density was calculated manually from the number of echoes returned from a single FM click in the echogram with a 25 ms window (Fig. 2-2). Less than 5 echoes was considered “low” echo density and greater than 5 echoes was considered “high” echo density. Further refining of this definition was not needed as nearly all environments were in the extrema of this definition.

Beam pattern effects and noise

In order to obtain information about the frequency response of a scatterer, without the benefit of a precisely known source signal, it was necessary to assume a consistent, undistorted emission from the whale. Evidence from on-axis recordings of click trains from other *M. densirostris* has shown that the frequency content in the main lobe of FM clicks is stable and relatively featureless in spectral content over the band of frequencies considered in this analysis (Johnson *et al.*, submitted). The same assumption can not be made for off-axis signals. Broadband signals emitted by dolphins have shown a distortion in the waveform and corresponding spectrum for small off-axis angles. Au (1993) attributes these off-axis distortions to the emitted signal radiating from different portions of a finite aperture and to internal reflections from the whale’s anatomy such as skull and air sacs. It is expected that similar distortions to off-axis clicks of other toothed whales, such as the one studied here,

would also occur. Therefore, it was necessary to constrain the echoes in this study to scatterers that were considered on-axis or nearly on-axis in order to take advantage of the smoothly shaped signal of this animal.

To localize the position of the scatterer within the whale’s forward beam, the polar angle, θ , is calculated from the difference in time of arrival between the two hydrophones using the relationship: $\theta = \arcsin(\tau c/d)$ where τ is the measured time delay between hydrophones, c is the speed of sound in seawater, and d is the distance between hydrophones. The error tolerance for θ is less than 1 degree. This angle, measured from the plane equidistant from the two transducers, only partially localizes the scatterer as the line of bearing from the whale to the scatterer has an ambiguity of 2π radians. However, the fact that the vast majority of echoes seen in the echograms (e.g. Fig. 2-2b) have a consistently decreasing TWT strongly suggests that most echoes, if not all, are coming from in front of the fast moving whale. The ambiguity is, therefore, believed to be a much smaller angle. An error due to angular offset of the tag with respect to the longitudinal axis of the whale, and presumably with the main beam, was visually observed during surfacing of the whale. Assuming equal distribution of echoes about the beam axis, this offset was corrected on each dive using the relationship: $\theta_{\text{beam}} = \theta_{\text{tag}} - \bar{\theta}_{\text{dive}}$, where angle of arrival, $\theta_{\text{subscript}}$, is measured from the axis of the reference frame noted in the subscript and $\bar{\theta}_{\text{dive}}$ is the mean zero offset of all echoes analyzed from a given dive.

In order to minimize effects due to the beam pattern off the main axis, acceptable echoes were limited to ± 4 degrees. Although the beam width for the *M. densirostris* is unknown, Zimmer *et al.* (2005) has shown that *Ziphius cavirostris*, a closely related beaked whale, has an estimated -3 dB beam width of 6 degrees. In line with the suggestion by Au *et al.* (1999), that a smaller head corresponds to a broader transmission beam, and considering the smaller size of the *Mesoplodon* (Mead, 1989) and similar centroid frequency (Zimmer *et al.*, 2005; Johnson *et al.*, submitted) it can be assumed that this whale has a slightly broader beam pattern. A conservative increase of 1 degree half beam width has been assumed.

Additionally, only echoes with an echo-to-noise ratio, ENR, of 8 dB were consid-

ered in the analysis in order to provide signal strength to differentiate structure in the received spectra from noise interference. It is believed that these constraints on ENR and AOA are sufficient to assume that structure in the spectra of the echoes is due primarily to the scattering physics of the ensonified object rather than a distortion of the received signal due to these interfering effects.

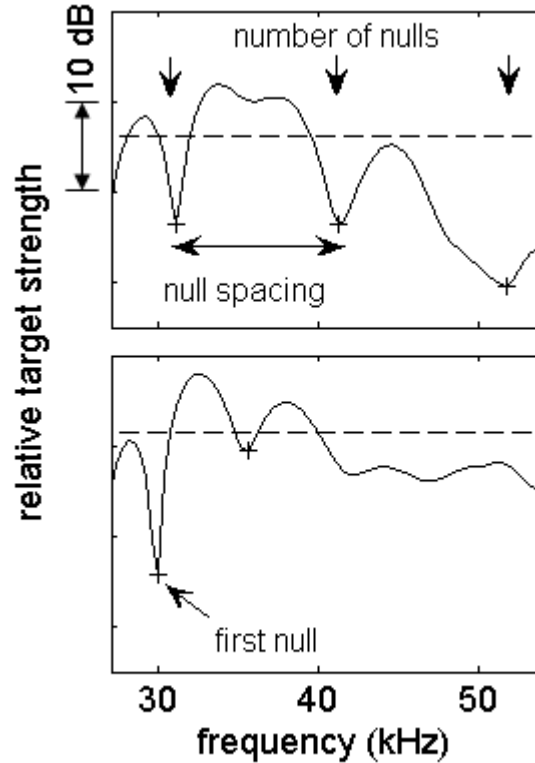


Figure 2-3: Example of automated structure analysis results. Plus signs indicate nulls and horizontal dashed lines indicate mean target strength of frequency band displayed. An example of the two criteria for a null are illustrated in the lower plot: (1) The dip near 42 kHz does not meet the criterion of 1 dB less than both adjacent peaks (2) The dip at 47 kHz does not meet the criterion of 3 dB less than the average of the two adjacent peaks.

2.4.2 Spectral classification

Acoustic scattering spectra of marine organisms are characterized by unique interference patterns specific to target size, shape, material properties, and orientation

(Stanton *et al.*, 1998b; Lavery *et al.*, 2002; Reeder *et al.*, 2004). In order to perform a quantitative, statistical analysis of the prey echoes compiled in this study, an algorithm was created to quantify the structure of the spectra. Once the echoes of interest were identified, the time series was filtered using a 20 to 70 kHz 4-pole Butterworth bandpass filter, and windowed using a 400 microsecond rectangular window. This result was then converted to a frequency spectrum using a Fourier transform.

The frequency band between 27 and 54 kHz was selected for analysis. This range falls within the -10 dB endpoints of the power spectrum of the transmitted signal and is limited to the range of frequencies where FM clicks have been shown to be nearly featureless as discussed in Sec. 2.2. Given the limited ENR of echoes selected for this study, three simple robust parameters were chosen to characterize the frequency response of the scatterers: (1) number of nulls, (2) location of first null, and (3) spacing of the first two nulls (Fig. 2-3). Nulls were identified by a greater than 3 dB difference between a local minimum and the average of two adjacent maxima. Nulls of less than 1 dB from either adjacent peak were discarded to minimize false detection of nulls. These limits were set so as to discriminate between nulls due to scattering phenomena and other sources of spectral structure such as variability in the source and ambient noise.

2.4.3 Target strength calculations

Estimated target strength of the scatterer was found using the active sonar equation (Urick, 1983).

$$TS = EL + 2TL - SL \quad (2.1)$$

For these calculations only target strength, TS , and the received echo level at the transducer, EL , were allowed to vary with frequency, f , as explained below. TL and SL are one-way transmission loss and source level respectively. All values are calculated in terms of dB re 1 μPa . The echo level is determined from the raw

time-voltage signal, $y(t)$ using the expression

$$EL(f) = 20 \log Y(f) - S \quad (2.2)$$

where $Y(f)$ is the discrete Fourier transform of $y(t)$ and S is the sensitivity of the tag in dB re $V/\mu Pa$.

Transmission loss, accounting for spherical spreading and absorption losses, was determined by the relation $TL = 20 \log r + \alpha r$, where r is one-way distance from transducer to scatterer and α is absorption loss. The frequency dependence of absorption was neglected as the effect on transmission loss over the short target distances and range of frequencies considered here was small (< 0.5 dB). Thus, alpha was considered a constant: $\alpha \simeq 11 \frac{dB}{km}$ @ 40 kHz (Urick, 1983).

Source levels have not yet been measured for this species; therefore, all target strength values are presented in relative terms. A constant source level, i.e. constant at each frequency within the band, was chosen to represent the featureless portion of the whale's transmitted signal. This notional source level, SL_k , was adjusted for variation in the apparent output of the transmitted click corresponding to each echo using the formula: $SL = SL_k + [AO - \overline{AO}]$, where AO is the apparent output of a specific click and \overline{AO} is the mean apparent output of all regular clicks associated with echoes analyzed. As discussed in Sec. 2.3, it is believed that this provides a reasonable method for estimating fluctuations in the source level and, therefore, improves the precision of relative target strengths.

Target strength, TS , can be further defined as the logarithmic measure of the backscattered energy and is given by

$$TS = 10 \log \sigma_{bs} \quad (2.3)$$

where σ_{bs} is the differential backscattering cross section. Mean target strength of an individual echo was found by averaging $\sigma_{bs}(f)$ over all frequency bins within the band of interest prior to logarithmic conversion.

Broadband acoustic signatures of whale prey

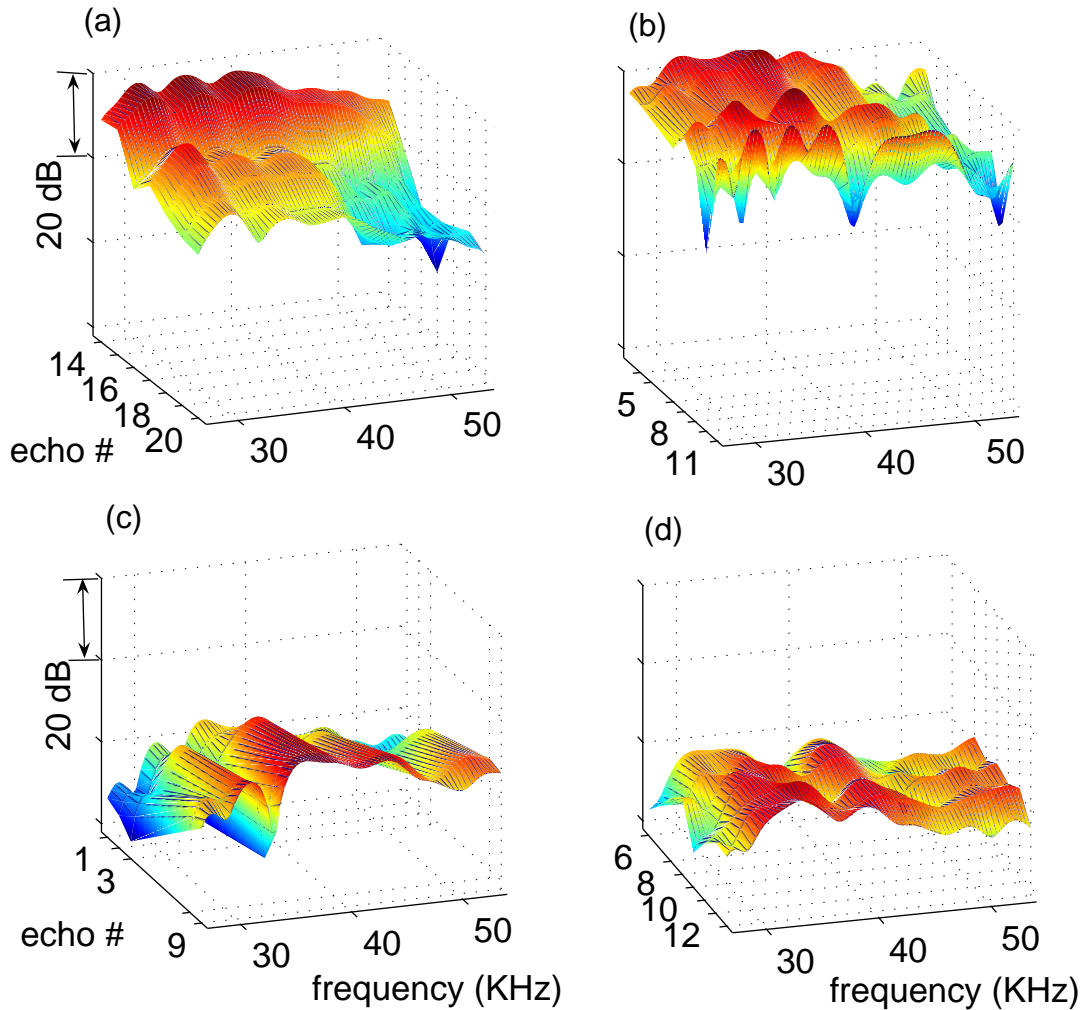


Figure 2-4: Broadband acoustic signatures of four prey selected by the whale. Each plot is comprised of frequency spectra of a series of echoes that make up one echo train. Plots only include spectra from echoes within each train that met the criteria discussed in Sec. 2.4.1. Echoes represented are identified by a tick mark on the “echo #” axis. Figures (a) and (b) show examples of high target strength prey found at deep depths (below 700 m) in low echo density environments. Figures (c) and (d) show examples of lower target strength prey found in shallower water (above 700 m) in high echo density environments.

2.5 Results

2.5.1 Echoes selected for analysis

A total of 89 buzzes were observed during the three dives analyzed indicating possible predation events. Of these, 47 were preceded by unambiguous echo trains that are believed to correspond to scattering from prey. The remaining buzzes were associated with either irresolvable echo trains due to a cluttered environment or no echo trains with sufficient ENR. Additionally, in the echograms of dive #3, where a high percentage of buzzes could not be correlated with echo trains, it is suspected that many echo trains existed but were obscured by reverberation from the bottom. The first echo of each train was discernable from background noise at varying TWT's equivalent to a distance to the scatterer of between 5 and 15 m. In each case the echo train terminated shortly before the start of the buzz at a distance of 3 to 5 m.

The 47 echo trains identified as prey selected by the whale contained a total of 426 discrete echoes. Of those 135 echoes from 30 different echo trains, met the criteria for sufficient ENR and for angle of arrival within $\pm 4^\circ$. In order to accumulate a sufficient number of non-selected echoes as a control, 92 echo trains from random scatterers, not selected as prey by the whale, were chosen. Of these 34 trains containing 102 echoes remained after following the same procedure. Distribution of the echoes over the three dives analyzed is shown in Table 2.1. Many more random, non-selected echo trains were required to obtain a similar sample size as they generally had fewer echoes in each train. This is likely due to the shorter length of time that these non-pursued scatterers remained within the whale's acoustic beam.

2.5.2 Echo classification

Characterization of echo trains for comparison

A comparison was conducted between echo trains from scatterers selected by the whale and a non-selected control set based on spectral complexity and relative target strength. The primary focus of this study is to investigate whether or not the whales

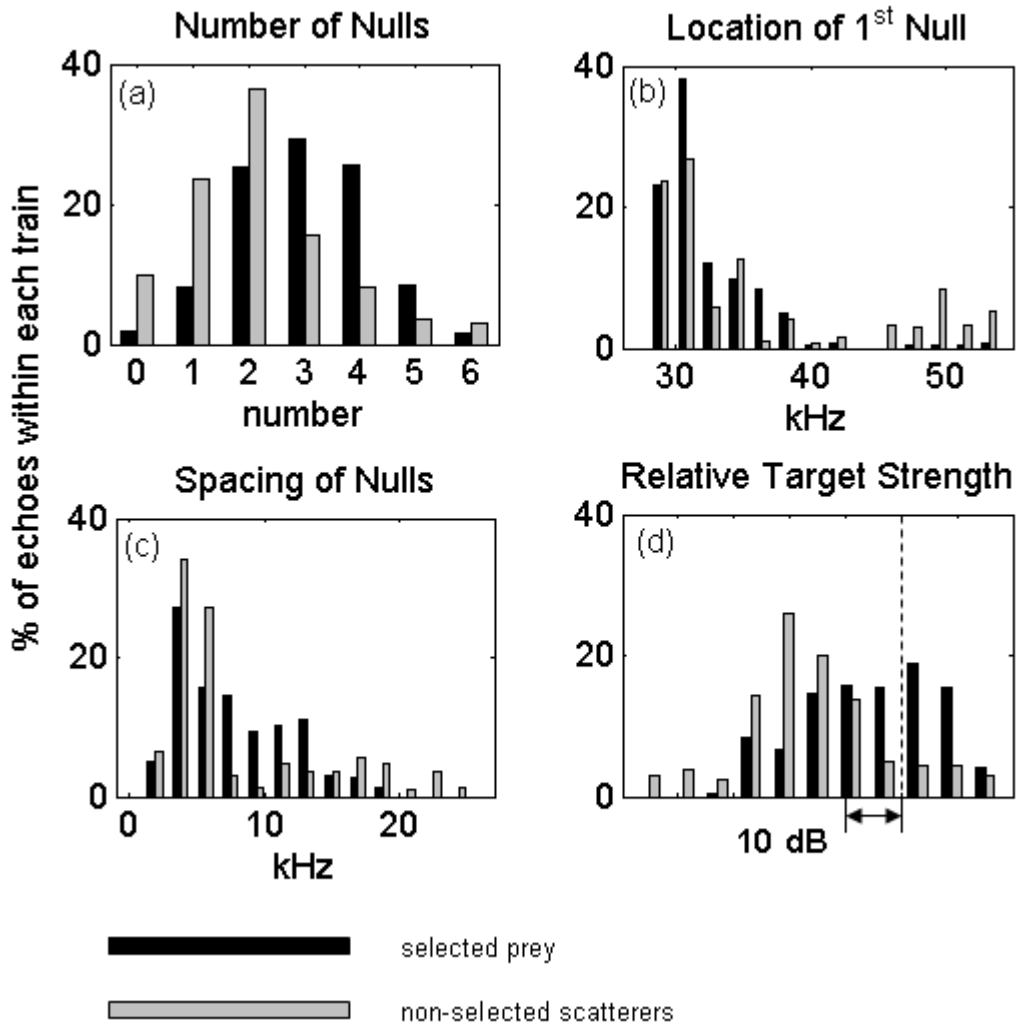


Figure 2-5: Normalized distribution of prey “selected” by the whale, and randomly chosen “non-selected” scatterers, i.e. not pursued by the whale as prey, (black and grey bars respectively) that contain a given characteristic: (a) number of nulls, (b) first null location, (c) spacing of first two nulls, and (d) relative target strength. Bins represent characteristics of a given echo within an echo train. Echoes are weighted by their fraction of the total number of echoes within a train. Distributions are normalized by the total number of echo trains (selected or non-selected). Vertical dashed line in target strength plot (d) represents absolute target strength value of -65 dB based on a source level of 200 dB.

Table 2.1: Distribution of echoes from selected and non-selected (in parenthesis) echo trains among three dives examined. Filtered echoes are limited to echo-to-noise ratio, ENR , of 8 dB and angle of arrival, AOA of $\pm 4^\circ$. Echo trains used in averaged results had a minimum of 2 echoes per train.

	echo trains	echoes
total identified		
dive 2	18 (36)	139 (276)
dive 3	9 (18)	77 (130)
dive 4	20 (38)	209 (177)
	47 (92)	425 (583)
filtered		
dive 2	7 (14)	30 (48)
dive 3	3 (14)	18 (47)
dive 4	20 (6)	87 (7)
	30 (34)	135 (102)

are discriminating between echoes with different characteristics. Since the spectra of discrete echoes from a single marine organism can vary significantly with small changes in the scatterer’s orientation (Reeder *et al.*, 2004), it is possible that distinct, but complementary information is obtained by the whale from multiple aspects of a single target. For these reasons the characteristics of individual echoes within each echo train, with no averaging, are considered in the statistical analysis performed on the data. Results presented here are shown as the number of echoes, as a percentage of the echo train in which they are contained, that exhibit a given spectral feature or target strength. The results are normalized by the total number of echo trains in the specific category, i.e. whale-selected group or non-whale-selected control group. It is believed that this method best reduces biases caused by the disproportionate length of some echo trains and also enables the classification of the echo trains according to one or more distinct features.

In addition to this method, two other statistical methods were used to analyze the echoes. One comparison was conducted on the echoes as a whole. In this method it was necessary to discard duplicate characteristics within an echo train to reduce the bias caused by echo trains of different lengths. The drawback of this method

was that, by removing redundant features within an echo train, key characteristics that may be used by the whale could be diluted through removal of an unrelated bias. Finally, an analysis was conducted by averaging the characteristics over each echo train. The effect of averaging is to smooth the frequency response patterns. In particular, sharp individual nulls in a discrete spectrum may become broad dips in an averaged frequency response. It is suspected that this approach may remove some subtle features of the echoes used by the whale in discriminating prey from other acoustic clutter. These concerns notwithstanding, good agreement was found in the primary results of all three methods. Only results of the first method, which present the data in the most raw form, are presented here.

Spectra

Results of the spectral analysis showed that significant structure exists, quantified by the number of nulls within the frequency band examined, in the frequency responses of many ensonified targets. As detailed in the data analysis section, it is believed that interference due to noise and beam pattern effects can be discounted as a major contributor to this structure. If noise were a significant contributing factor to the spectral structure, a trend towards a lower ENR for echoes containing more nulls would be expected as these echoes would be more susceptible to this interference. However, a comparison of number of nulls and ENR over all angles of arrival did not show such a trend. Instead the comparison showed only a 3 dB decrease in echo-to-noise ratio from 0 to 2 null targets and, most notably, a flat trend from 2 to 6 nulls. Furthermore, no correlation was found between number of nulls and angle of arrival, θ_{beam} . This supports the assumption that the constraint of a narrow range of arrival angles has removed any distortion effects due to the angular offset within the whale's sonar beam.

Figure 2-5a shows a comparison of the number of nulls in the frequency spectra of echo trains selected by the whale and non-whale-selected echo trains from all dives examined. One can see that there is a bias, in the echo trains from scatterers selected as prey, towards more highly structured returns (selected mean: 3.06, non-selected

mean: 2.12). A t -test showed that the difference was significant ($t = 2.803$, $df = 63$, p -value = 6.72×10^{-3}). Notably, less than 2% of the selected echo trains were characterized by a featureless echo (i.e. an echo with no nulls), whereas nearly 10% of the non-selected echo trains were composed of such echoes. These results are contrary to that which would be expected if echo structure was primarily due to effects of the off-axis beam pattern. Non-selected targets are more slightly more likely to fall on the edge of the transmitted beam pattern, $\theta_{\text{beam}} \geq \pm 3deg$, (non-selected: 24.5%, selected: 20.0%), probably because they are not being actively pursued by the whale. However, a bias in structure content due to location in the beam, which would be expected if beam pattern effects were strong, is not seen.

A comparison of the different structure features between the selected and non-selected echo trains was less revealing. Figure 2-5 (b and c) compare the the whale-selected and non-whale selected distributions of first null locations and spacings of the first two nulls, respectively. These results did not appear to have normal distributions and a Kolmogorov-Smirnov test showed no significant difference in the distributions (null location: $k = 0.290$, p -value = 0.131, null spacing: $k = 0.232$, p -value = 0.381). The spacing of the nulls did appear to have a bi-modal (selected) and multi-modal (non-selected) distribution.

Target strengths

Echo trains selected by the whale are composed of echoes that have a target strength distribution that is shifted approximately 18 dB higher than non-selected echo trains (Fig. 2-5d). A Kolmogorov-Smirnov test rejected the null hypothesis that the two samples were from the same distribution ($k = 0.400$, p -value = 7.22×10^{-3}). It is also observed that echo trains from selected prey showed wide echo to echo variation in target strength with 60% containing echoes that varied by 9 dB while 17% contained echoes varying by at least 15 dB. Non-selected echo trains had less variability with only 26% of echo trains having a 10 dB variation and 15% varying by at least 15 dB. This difference in variability between selected and non-selected echo trains may be a factor of the fewer number of echoes, on average, in the non-selected echo trains.

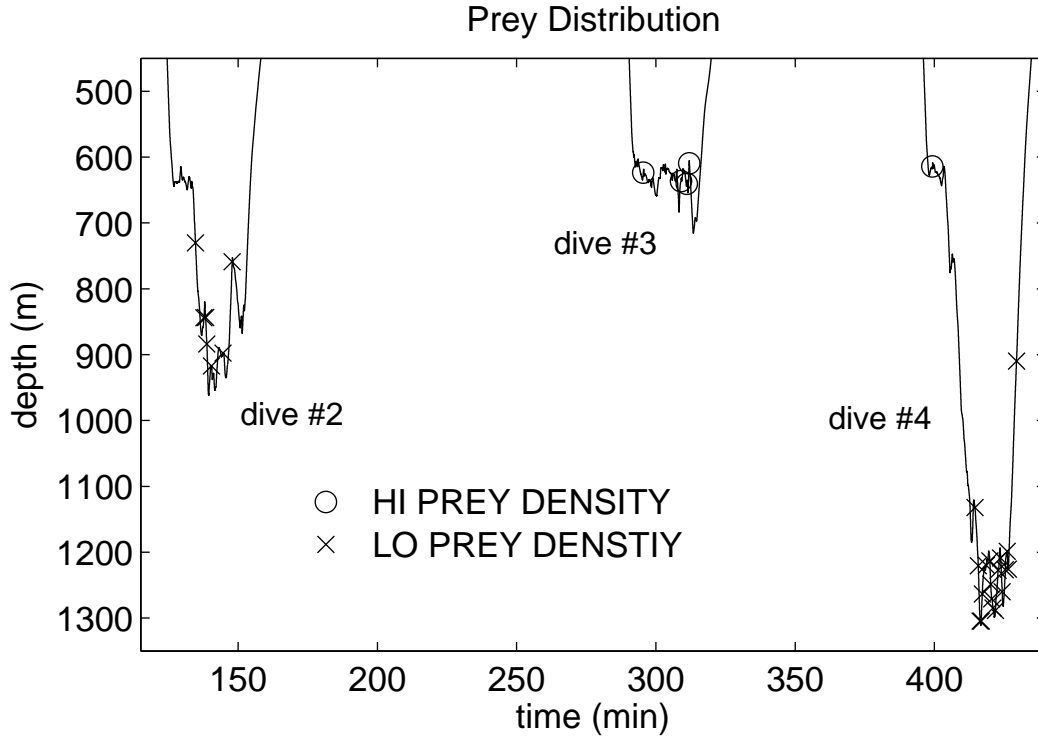


Figure 2-6: Depth distribution of prey categorized by echo density. Depth is truncated above 450 m as no predation events were found at shallower depths.

2.5.3 Comparison of echo characteristics between two groups of prey

Echo characteristics of two groups of prey, which were separated by depth and differed in aggregation density, are compared. It is suspected that two distinct prey categories can be defined by comparing discrete backscattering by prey in a deep, low echo density aggregation with prey in a shallow, high echo density aggregation. Echo density, in regions where the whale hunted, varied widely during the three dives (Fig. 2-2). Prey aggregations on dive #2 and #4 were characterized by low density while dive #3 was nearly exclusively high echo density. The two suspected prey categories were separated spatially in the water column with the high density group in water shallower than 700m and lower density group found at greater depths (Fig. 2-6).

In the shallow, high echo density aggregation, differences in the number of nulls between selected and non-selected targets is shown to not be significant by a Kolmogorov-

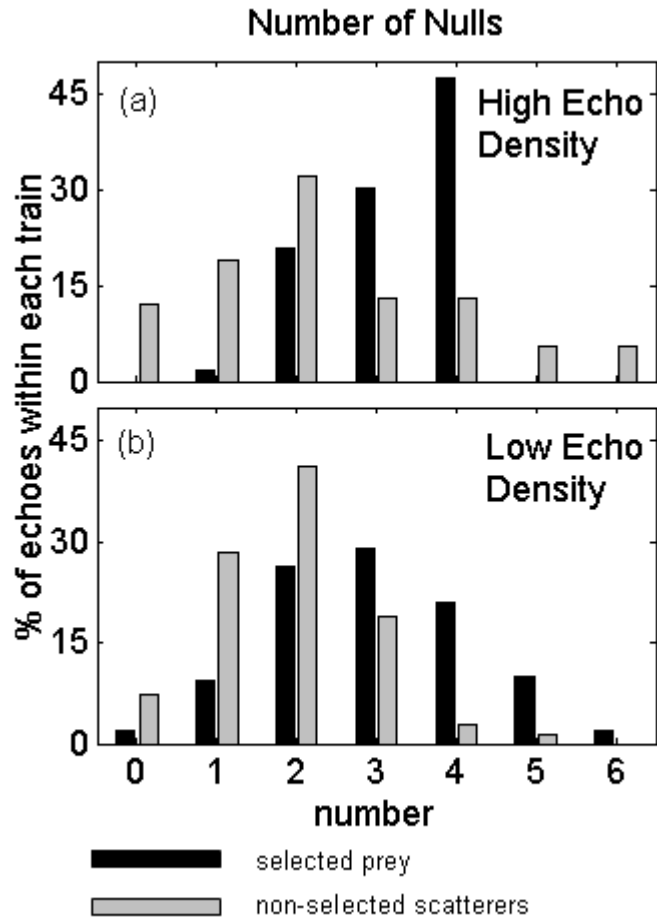


Figure 2-7: Spectral content in frequency responses of prey selected by the whale and non-whale-selected scatterers (black and grey bars respectively) in: (a) shallow, high echo density aggregations, and (b) deep, low echo density aggregations. Weighting and normalization are identical to Fig. 2-5.

Smirnov test ($k = 0.447$, $p\text{-value} = 0.318$) and may have suffered from small sample size (Fig. 2-7a). However, as in the combined results of all prey targets, discussed in Sec. 2.5.2, the targets selected by the whale in the low echo density aggregation were characterized by more highly structured echoes than the control group of non-selected targets (Fig. 2-7). A t -test showed that the difference in means (selected: 2.96 nulls, non-selected: 1.85 nulls) was significant ($t = 3.186$, $df = 40$, $p\text{-value} = 2.80 \times 10^{-3}$) Other spectral characteristics were also inconclusive here due to the small sampling

size available.

The target strength distribution provided further information about these two scattering groups. The target strength distribution between selected and non-selected echo trains in both echo density environments were heavily overlapping (Fig. 2-8). No significant difference was found using Kolmogorov-Smirnov tests in either case (high echo density: $k = 0.178$, p -value = 0.999; low echo density: $k = 0.340$, p -value = 0.140). However, when scatterers from the two environments are compared it can be seen that there is at least a 15 dB shift in the target strength distributions.

2.5.4 Comparison between echo characteristics and scattering predictions/observations

Target strength variability

In Sec. 2.5.3. a significant difference in the target strength distribution is shown between a shallow, high echo density aggregation and a deep, low echo density aggregation. Using a simple, straight finite cylinder model for weakly scattering marine organisms of length L , it is seen that in the geometric scattering region target strength varies as $10 \cdot \log(L^2)$, (Stanton *et al.*, 1993, 1994). This first order approximation can be used to estimate a ratio of the prey lengths from the difference in target strengths. For broadside scattering from two organisms of roughly the same aspect ratio and material composition, a 15 dB difference in target strengths correlates to a length factor of approximately 5.5. The fact that this whale dives to significantly greater depths, i.e. an additional 500 to 600 m, to pursue a type of prey found in less dense aggregations is counterintuitive. However, the possibility that the prey found at depth are significantly larger may be one explanation for this behavior.

Effects of orientation

In another study an acoustic scattering model for squid has been developed. This is based on a weak-scattering theory using high resolution spiral computerized tomography (SCT) scans. Predictions of target strengths from small squid have been made

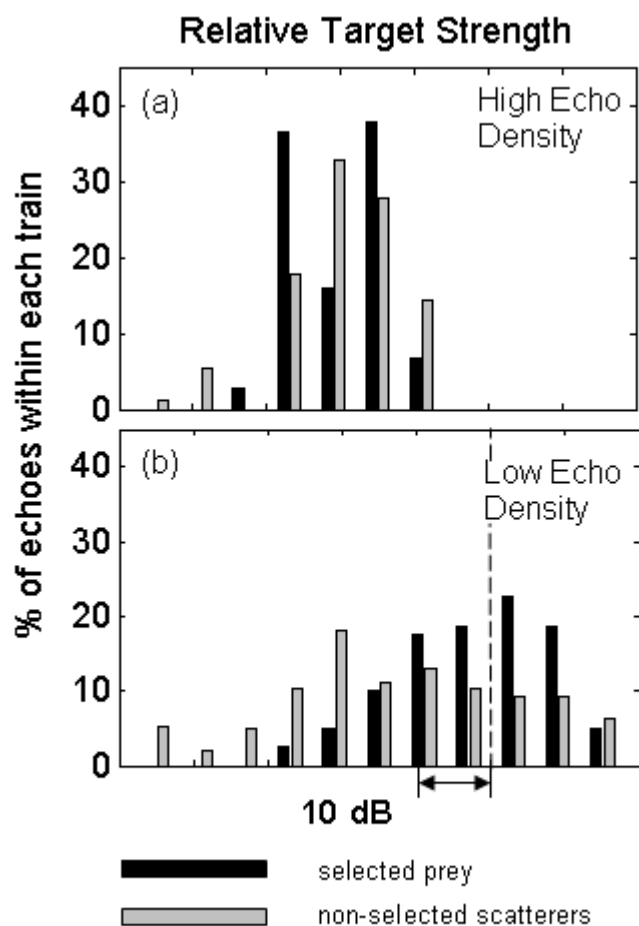


Figure 2-8: Reduced target strength distribution of prey selected by the whale and non-whale-selected scatterers (black and grey bars respectively) in: (a) shallow, high echo density aggregations, and (b) deep, low echo density aggregations. Vertical dashed line represents absolute target strength value of -65 dB based on source level of 200 dB. Weighting and normalization are identical to Fig. 2-5.

over a range of angles and orientation. In the analysis of whale-prey echoes, significant ping-to-ping variability in both structure content and target strength if found to exist within some echo trains selected by the whale (Fig. 2-4a and b). Because the transmitted signal of the whale has been constrained to near on-axis signals, variations presumably relate to the orientation of the scatterer relative to the incident sound wave. Modeling predictions for squid show a similar variability. The interference pattern and magnitude of the frequency response are highly affected by changes

in the aspect of the scatterer with respect to the incident sound wave. Measured broadband scattering from fish have shown similar results with changes as small as 5 degrees dramatically changing the backscattered frequency response (Reeder *et al.*, 2004).

2.6 Discussion

The characteristics of broadband echolocation signals have been studied through data obtained, *in situ*, by a recording device mounted on a foraging Blainville's beaked whale. By setting stringent criteria on the echoes analyzed and, in part, due to the opportunely smooth spectrum of the *M. densirostris*' emitted signal, the spectral characteristics of the prey's frequency responses can be analyzed over a limited frequency range and relative target strengths can be estimated.

Significant structure, resembling the type of interference patterns observed from marine organisms in modeling and laboratory experiments, exist in the frequency spectra of prey echoes measured in this study. It has been concluded that structure contained within the frequency responses of scatterers is consistent with, and most likely due to, interference from multiple wave interactions incurred by the morphology, material properties, and orientation of the scatterer.

A combination of whale depth and echo density was combined with the scattering results to show that it is likely that the whale preyed upon at least two different types of organism with different target strength distributions. This whale hunted a low target strength population found in high density aggregations between depths of 600 and 650 m. Higher target strength prey were found at various depths below 700 meters in low echo density environments. In neither case was a significant difference found in the target strength distributions between prey selected by the whale and a control group of non-whale-selected scatterers. This suggests that the target strength of a scatterer is not the whale's sole means of discriminating between prey and non-prey targets. It is significant that, for at least the low echo density case, this animal appeared to favor targets that display a higher degree of structure within

their frequency responses. It is not possible to confirm, however, that this whale is using specific structural features, such as null location or spacing, in recognizing or classifying specific prey items.

Finally, an explanation has been proposed as to why this large marine predator chooses to dive to significantly deeper depths to hunt less dense populations of prey. Scattering theory for weakly scattering, non-swimbladder bearing marine organisms suggests that the higher target strength organisms found at depth could be 5 to 6 times the size of prey hunted in shallower water, thus giving the animal an incentive to expend the energy required to dive to greater depths.

Chapter 3

Acoustic scattering by weakly scattering shelled objects: Application to Squid¹

3.1 Introduction

A model has been developed, based on the distorted wave Born approximation (DWBA), to predict acoustic scattering from arbitrarily shaped, arbitrarily inhomogeneous, weakly scattering volumes. Although the DWBA formulation, in principle, can account for 3-D material property inhomogeneities, significant obstacles are encountered when applying this model to a randomly inhomogeneous object. In the Born approximation the amplitude and phase of the incident wave are only dependent on the position of the wave front with respect to some arbitrary origin and the material properties of the surrounding medium. This is due to the general assumption that the incident wave is unmodified by the weakly scattering body. In contrast, the DWBA is a modification to the Born approximation in which the wavenumber inside the scattering volume is determined by the material properties within the body (Stanton *et al.*, 1993). Thus, the phase of the wavefront, at any point in the volume,

¹This chapter is based on an article to be submitted to the Journal of the Acoustical Society of America (Jones *et al.*, in prep.a)

is dependent both on the distance traveled by the incident wave and any sound speed variations encountered along the path traveled.

As discussed in Ch. 1, the DWBA has been applied to homogeneous scattering volumes and volumes with material properties that vary only in one dimension. In these cases the DWBA formulation can be applied directly, either to the body as a whole or, in the axially varying case, to each cross section separately assuming normal incidence of the sound wave. The primary advance made in this study is correctly accounting for the phase of the incident wave as it travels through an inhomogeneous medium. The numerical incorporation of this method uses a ray trace component to track the phase at every position within the scattering volume. A two part algorithm calculates phase and amplitude for every discretization before integrating over the entire volume. Application of this DWBA ray-tracing model to squid is discussed in detail.

Although relatively little work has been published on acoustic scattering models of squid there is interest in this research from two areas. The first is commercial fisheries. As a fast growing but short-lived species, squid are particularly vulnerable to overfishing (Goss *et al.*, 2001). Acoustic stock assessments can be used to complement more traditional techniques such as trawl surveys and fishery catch analyses by rapidly surveying large volumes of water and providing real time population assessments (review by Starr and Thorne (1998)). Understanding the factors that influence sound scattering from squid is clearly essential for reliable surveys of this type. Secondly, there is increasing interest in the predator-prey relationship between echolocating marine mammals and squid. Beaked whales, for instance, hunt squid using broadband, ultrasonic sonar (Johnson *et al.*, 2004; Madsen *et al.*, 2005). Scattering models that help define the dominant scattering mechanisms of squid may elucidate factors that are exploited by the whales in discriminating between prey and non-prey.

The DWBA ray-tracing model is applied to long-finned squid, (*Loligo pealeii*). Density and sound speed measurements of squid suggest that these invertebrates are well suited to modeling as weak scatterers (Mukai *et al.*, 2000; Kang *et al.*, 2004; Iida *et al.*, 2006). Accordingly, previous models of squid use the exact liquid prolate spher-

oid model (LPSM) and the DWBA formulation, also using prolate spheroid geometry (Arnaya and Sano, 1990b; Mukai *et al.*, 2000). These models assume homogeneous material properties within the scattering volume. In this study high-resolution spiral computerized tomography (SCT) scans have been used to obtain 3-D morphology of squid. Unlike previous DWBA models of squid, the DWBA ray-tracing model incorporates the complex mantle structure by differentiating between seawater filled cavities and the squid’s body. Material property variation due to internal organs, however, is not included in this study. Predictions are compared with published results of both anesthetized, tethered squid and live, freely swimming squid.

Application of the DWBA ray-tracing model is presented in two parts. First, to validate the model, it is applied to simple geometric shapes of both homogeneous and inhomogeneous material composition. Target strength predictions are compared with solutions to modal-series-based formulations, and existing DWBA scattering models defined in Sec. 3.2. Acoustic scattering predictions, given in Sec. 3.4.1, are calculated for simple geometric objects with variations in material properties, shell thickness, and orientation. Second, the DWBA ray-tracing model is applied to squid of the species *L. pealeii*. In order to compare scattering predictions with actual scattering measurements, the model is extended to a second species of squid *T. pacificus* by digitally scaling the 3-D morphological measurements of squid used in the model. Comparisons of predicted target strengths with published target strength data for this species are shown in Sec. 3.4.2.

3.2 Theory

3.2.1 Basic definitions

Acoustic scattering from an object in the far field is described in terms of the amplitude of the incident sound wave, P_0 , and the scattering amplitude, f ,

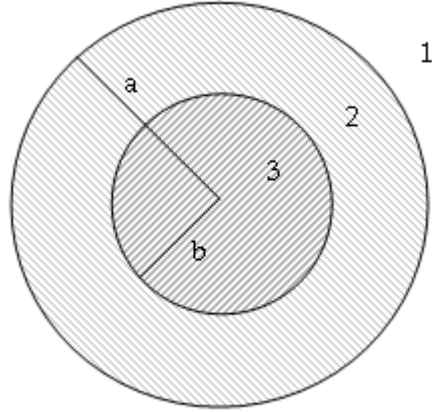


Figure 3-1: Bisection of spherical shell or cross section of cylindrical shell. Indices 1-3 correspond to fluids of different material properties (i.e. sound speed, c_i , and density, ρ_i , $i = 1, 2, 3$). The radii a and b are the outer and inner shell radii respectively such that $(a - b)/a$ corresponds to fractional shell thickness, τ .

$$P_{scat} = P_0 \frac{e^{ik_1 r}}{r} f \quad (3.1)$$

where, r is the distance from the object to the receiver. The acoustic wavenumber of the surrounding medium, k_1 , is defined as $2\pi/\lambda$, where λ is the acoustic wavelength.

Target strength is the logarithmic measure of the backscattered energy, expressed in decibels, dB, relative to m^2 .

$$TS = 10 \log \sigma_{bs} \quad (3.2)$$

where $\sigma_{bs} = |f_{bs}|^2$ is the differential backscattering cross section and f_{bs} , or backscattering amplitude, is f evaluated in the backscattered direction. Mean target strength is found by averaging σ_{bs} prior to logarithmic conversion as $\langle TS \rangle = 10 \log \langle \sigma_{bs} \rangle$.

In order to compare scattering from objects that are similar in proportion but of different overall size, reduced target strength, RTS , is often used. For a sphere or

spherical shell of outer radius a (Fig. 3-1) it is given by

$$RTS = 10 \log \frac{\sigma_{bs}}{\pi a^2} \quad (3.3)$$

In the case of elongated objects such as cylinders or cylindrical shells of length L reduced target strength is given by

$$RTS = 10 \log \frac{\sigma_{bs}}{L^2} \quad (3.4)$$

For the case of scattering from squid, the length L is replaced by dorsal mantle length, L_{ml} . Additionally, due to the lack of published data on mean mantle widths, from which mean radii for squid could be derived, the non-dimensional term $k_1 L_{ml}$ is used instead of the more commonly used $k_1 a$.

3.2.2 DWBA-based scattering models

The Born approximation is derived for weakly scattering bodies in which the pressure field inside a scattering volume is approximated by the unperturbed, incident field. The approximation is valid when the amplitude of the scattered wave is much smaller than the incident wave (Morse and Ingard, 1968). Due to its volume integral form this approximation may be used for arbitrarily shaped scatterers with any orientation with respect to the incident sound wave. The distorted wave Born approximation (DWBA) involves replacing the incident wavenumber vector inside the integral with the wavenumber vector of the internal medium. It is this modification that accounts for phase change of the sound wave due to material property inhomogeneities within the scattering volume. The DWBA formulation is valid for the entire range of frequencies and all angles of orientation. It is given by

$$f_{bs} = \frac{k_1^2}{4\pi} \int \int \int_v (\gamma_\kappa - \gamma_\rho) e^{2i\vec{k}_v \cdot \vec{r}_v} dv \quad (3.5)$$

Material properties are expressed in terms of compressibility, κ , and density, ρ , or the commonly used ratios of density, $g_v = \rho_v/\rho_1$, and sound speed, $h_v = c_v/c_1$, given

here by

$$\gamma_\kappa = \frac{\kappa_v - \kappa_1}{\kappa_1} = \frac{1 - g_v h_v^2}{g_v h_v^2} \quad (3.6)$$

$$\gamma_\rho = \frac{\rho_v - \rho_1}{\rho_2} = \frac{g_v - 1}{g_v} \quad (3.7)$$

In all cases the subscript “1” indicates parameters of the surrounding medium and the subscript “ v ” indicates parameters within the scattering volume. Accordingly, the wavenumber in the external medium is the constant k_1 , while the wavenumber vector within the volume is \vec{k}_v . Throughout this paper, when a model formulation is applied to a scattering problem, the subscript “ v ” takes on the integers “2, 3, ...” corresponding to given material property parameters of that region within the volume. For example, in the region designated by “3” in Fig. 3-1 the sound speed ratio, g_v , becomes $g_3 = \rho_3/\rho_1$.

It has been noted that the DWBA formulation will have phase errors for cases where the internal volume has inhomogeneous material properties or when the wave passes through part of the body, into the surrounding medium, and back into the body. However, the phase can be accurately calculated at each point in the volume by piecewise integration of the exponential phase term (Stanton *et al.*, 1998a). It is this advance, accomplished numerically and detailed in Sec. 3.3, which is the motivation for this work.

For straight, finite cylinders with homogeneous material properties, Eq. (3.5) can be solved analytically (Stanton *et al.*, 1998a). This result is used to test the DWBA ray-tracing model over varying orientations of the scattering volume with respect to the incident acoustic wave. This model is termed the *DWBA solid, finite cylinder model* throughout this paper and is given by

$$f_{bs} = \frac{k_1 k_v a^2 L}{2} (\gamma_\kappa - \gamma_\rho) e^{-iLk_v \sin \theta} \frac{J_1(2k_v a \cos \theta)}{2k_v a \cos \theta} \frac{\sin(k_v L \sin \theta)}{k_v L \sin \theta} \quad (3.8)$$

where J_1 is the Bessel function of the first kind, k_v is the amplitude of the wavenumber within the volume, and θ is the angle of the incident wave measured

from the longitudinal axis of the cylinder ($\theta = 0$ is normal incidence).

3.2.3 Exact modal-series-based scattering models

The primary purpose of this paper is to describe a DWBA-based ray tracing model that can accurately account for material property inhomogeneities within a scattering volume. In order to validate the model for an inhomogeneous object, comparisons are made with two analytic solutions for scattering from simple geometric, shelled, and hence inhomogeneous, objects. The two modal-series-based formulations presented here test the model over a range of frequencies and shell thicknesses.

The wave equation can be separated and solved exactly for a limited number of simple shapes (e.g. spheres, infinite cylinders, prolate spheroids, etc.). In this section scattering models are presented for fluid-filled, fluid spherical and finite cylindrical shells. The term “fluid” implies that the formulation does not include shear waves. The modal series solutions for these simple geometric volumes are derived by separating the wave equation in spherical and cylindrical coordinate systems, respectively, and applying two boundary conditions at each interface: continuity of pressure and continuity of radial velocity. Though these solutions are straight forward to derive, the resulting coefficients for these particular cases are not known to have been documented previously and are presented in appendix A.

Fluid-filled, fluid spherical shell

The far field, modal-series-based solution to the wave equation for a fluid-filled, fluid spherical shell in the backscattered direction is expressed as

$$f_{bs} = \frac{i}{k_1} \sum_{n=0}^{\infty} (2n+1)(-1)^n A_n \quad (3.9)$$

where, A_n is the modal series coefficients and is given in appendix A.

Fluid-filled, fluid cylindrical shell of finite length

The finite length cylindrical shell approximation uses the coefficients of the modal series solution for an infinitely long cylinder. While the exact modal series solution for infinite cylinders is valid for all angles of orientation, the finite cylinder approximation neglects end effects and is, therefore, valid only near broadside. Accordingly, this formulation is only applied at normal incidence to test the DWBA ray-tracing model over a range of frequencies.

Stanton (1988), related the scattering amplitude of a finite cylinder to that of an infinite cylinder using a volume flow per unit length approximation. These equations can, likewise, be applied to a finite length cylindrical shell. Applying the backscatter condition to the equation for a finite fluid-filled, fluid cylindrical shell results in

$$f_{bs} = \frac{-iL}{\pi} \sum_{n=0}^{\infty} -\epsilon_n (-1)^n B_n \quad (3.10)$$

where, B_n is the modal series coefficients to the *infinite* length fluid-filled, fluid cylindrical shell and is given in appendix A. The term ϵ_n is the Neumann number ($\epsilon_0 = 1$, $\epsilon_n = 2$ for $n = 1, 2, 3, \dots$).

3.3 Materials and methods

3.3.1 Animals studied

Two species of squid are discussed in this article. High resolution morphometry are taken of a locally available species, the long-finned squid, *Loligo pealeii*, while published target strength data is available for a second species, the Japanese common squid, *Todarodes pacificus*. Scattering predictions are calculated using the DWBA ray-tracing model, which makes use of high resolution morphology of *L. pealeii*. Additionally, predictions are made based on a version of this squid's 3-D morphology scaled to match the aspect ratio, i.e. width to length ratio, of a *T. pacificus* and compared with published data.

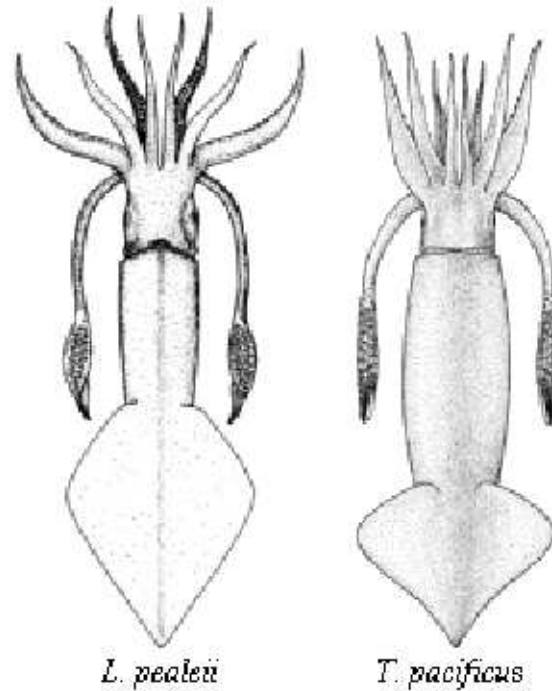


Figure 3-2: Sketches of the species of squid discussed in this article (Roper *et al.*, 1984). The *L. pealeii*, shown on the left, is the littoral species found near Woods Hole, MA, from which high resolution morphometry was obtained using SCT scans. The *T. pacificus* shown on the right, a pelagic species found in the western Pacific Ocean, has a larger aspect ratio (width-to-length ratio). Published data from experiments involving this species are used to compare with DWBA ray-tracing model predictions.

Long-finned squid, *Loligo pealeii*

L. pealeii specimens, obtained from the Marine Biological Laboratory, were selected due to ease of availability and well documented details of its anatomy. This coastal species of squid has a long, slender body and a large fin in proportion to its mantle length as implied by its common name. The commercial importance of *L. pealeii* comes from fishing and biological research (Roper *et al.*, 1984).

Japanese common squid, *Todarodes pacificus*

T. pacificus are an oceanic squid with a muscular, moderately slender body and a relatively short fin. Although these squid have a larger aspect ratio than *L. pealeii*, the two species are broadly similar (Fig. 3-2). *T. pacificus* are of high commercial

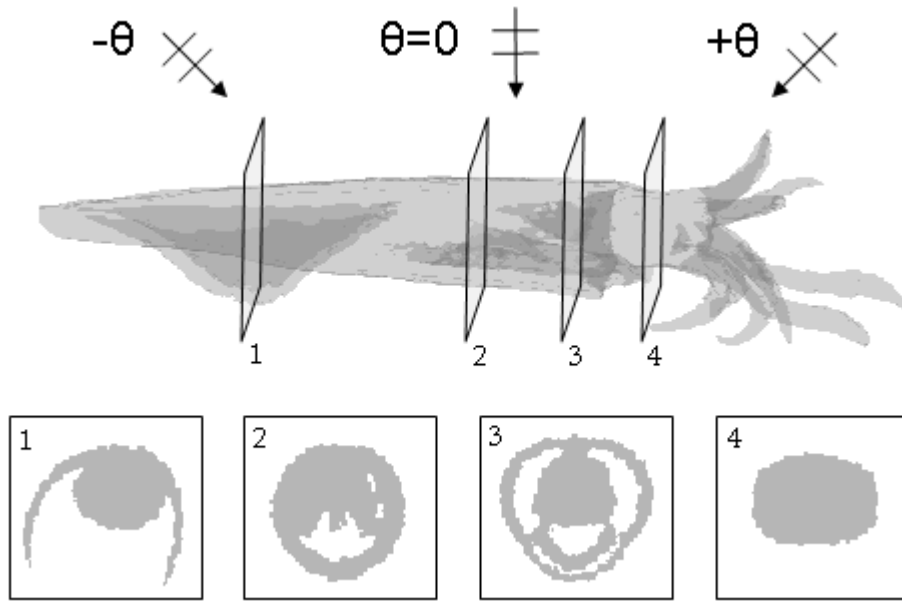


Figure 3-3: Volume rendering composed of SCT scan images of *L. pealeii* (in semi-transparent grey-scale) and four binary cross sections, M_i , showing the fin (1), mantle cavity (2,3), and neck (4). In the cross sections grey indicates squid body and white indicates surrounding seawater and seawater filled cavities. Arrows show the orientation of the squid with respect to an incident sound wave ($-\theta$ is head down, $+\theta$ is head up, and $\theta = 0$ corresponds to normal incidence).

interest to Japan and support the largest squid fishery in the world (Roper *et al.*, 1984; Sakurai *et al.*, 2000).

Squid material properties

Reliable acoustic scattering predictions require accurate values of sound speed and density of the scatterer. This is especially true of weakly scattering organisms whose material properties may vary from seawater by only a few percentages (Chu *et al.*, 2000). Published literature on squid material properties is limited (see table 3.1). However, some recent measurements provide useful information for this study. Kang *et al.* (2004), measured average density and sound speed of anesthetized squid in seawater. Their sound speed estimates, as compared to previously reported values, show better agreement with measured target strength data when used as parameters in a Kirchhoff ray mode (KRM) model. Iida *et al.* (2006), recently obtained values

Table 3.1: Material properties of squid from published sources. Values given as a ratio of squid material properties to those of seawater in the same publication.

reference	material	g	h
Hashimoto and Maniwa (1952, in Japanese)	whole squid	–	1.007
Mukai <i>et al.</i> (2000)	whole squid	1.025	–
Kang <i>et al.</i> (2004)	whole squid	1.028	1.04
Iida <i>et al.</i> (2006)	mantle tissue	1.043	1.053

for sound speed and density through squid mantle tissue. These values for g and h are higher than reported for whole squid. This is expected, however, as these measurements are for a single tissue type whereas the whole squid measurements are average values of sound speed and density through both the squid tissue and the seawater-filled mantle cavity. In light of these results, the values given by Iida ($g = 1.043$ and $h = 1.053$) were used in the DWBA ray-tracing model to represent the non-seawater filled regions of the squid’s body (i.e. tissue, organs, etc.). Seawater filled cavities were given values of 1 for g and h .

3.3.2 High resolution morphometry of squid: SCT scans

Spiral computerized tomography (SCT) scans were taken of a live, anesthetized squid at the Marine Research Facility at the Woods Hole Oceanographic Institution (Fig. 3-3). Spiral CT scanners measure data in a helical manner by advancing the body continuously through the scanning aperture for each 360° rotation. Cross sections are then reconstructed by interpolation into 2-D images with each pixel containing the x-ray attenuation in Hounsfield units, HU, (Hofer, 2000).

The squid measured in this study was anesthetized in a 1% ethanol seawater solution. During scanning the animal was suspended vertically in seawater to minimize distortion of body shape caused by laying the animal, unsupported, on a hard surface. Contrast agent was added to the seawater to help distinguish between x-ray attenuation of the solution and the squid body. Scans were taken by a Siemens Volume Zoom, four-slice SCT scanner using pitch and collimator settings of 2 mm and 1

mm respectively. Images of 512×512 pixels were reconstructed from the data using 0.5 mm slice thickness. Individual pixel size was 0.5078×0.5078 mm. Images were later resized on separate mathematical software using bicubic interpolation such that all pixels represent one cubic volume element, or voxel, with dimensions, l_{vs} equal to $0.5 \times 0.5 \times 0.5$ mm. In this way dimensional ratios are preserved in the image rotations discussed in the next section.

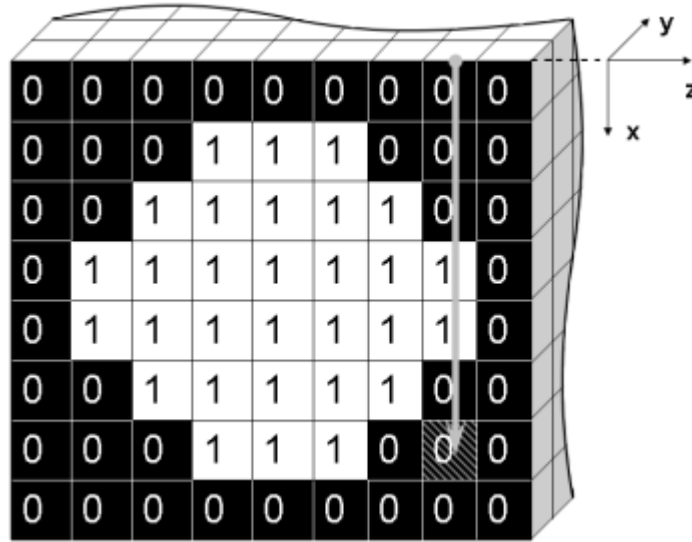


Figure 3-4: Ray trace illustration through inhomogeneous volume. Each differential element is labeled with an integer that indicates the specific fluid type. The phase change, due to sound speed of the fluid and distance traveled, is calculated in the x direction. Each differential element is assigned a phase change. The total one-way phase to any individual volume element, or voxel, is the cumulative sum of phase changes in the x direction from the origin to that point.

3.3.3 Numerical implementation of the DWBA ray-tracing model

Ray tracing and volume integration

This model, which numerically computes the DWBA volume integral, is based on discretizing the scattering volume, S_v . This volume is composed of “ l ” cross-sectional matrices, M . Each element of the matrix, M , represents one volume element, or *voxel*,

and is assigned an integer value depending on the material properties of that voxel. The matrices, M^l , are not directly incorporated into the summation, but instead, as a single 3-D matrix, they provide a map of the regions of various material properties within the volume. Although only two fluid types are used to represent scattering volumes in this study, it should be noted that this model can be applied to volumes containing any arbitrary variation of material properties.

In order to accurately track the phase of a sound wave as it is transmitted through an inhomogeneous scattering volume, it is necessary to incorporate a ray trace component. This algorithm is used to calculate the phase of the incident wave at each voxel. The computed phase term numerically represents the piecewise integration of the exponential phase term in Eq. (3.5). Since the backscattered case is considered here, only the one-way phase change is found, which is then simply doubled to find the full phase term.

The task of calculating phase change through the scattering object is begun by digitally rotating the volume matrix, S_v , such that the incident wavenumber vector, \vec{k}_1 , is orthogonal to the new cross sections \tilde{M}^l . All rotations are accomplished using “nearest neighbor” interpolation, thus preserving the integer value of each matrix element. The benefit of this rotational approach is in greatly simplifying the ray trace to a one dimensional problem in the x direction (Fig. 3-4). Once the rotations are complete, the differential phase change, which depends on the locally assigned sound speed, is calculated for each voxel. The total one-way phase change to each volume element is then found as the cumulative summation of these differential phase changes from the origin to this voxel in the x direction.

Finally, a search routine creates a linear index of all voxels within the rotated volume, \tilde{S}_v , assigned a particular material property and matches the appropriate amplitude term with the round trip phase term. Thus, the analytical expression given in Eq. (3.5) becomes

$$f_{bs} = \frac{k_1^2}{4\pi} \sum_{l=1}^{N_z} \sum_{j=1}^{N_y} \sum_{i=1}^{N_x} (\gamma_\kappa - \gamma_\rho)_{ij}^l e^{2i\varphi_{ij}^l} dv \quad (3.11)$$

where dv is the product of the differential distances, dx , dy , and dz , and the phase term, φ_{ij}^l , is a cumulative summation of the phase change, in the x direction, and is given by

$$\varphi_{ij}^l = \sum_{q=1}^i k_{qj}^l dx \quad (3.12)$$

Numerical issues

The accuracy of digitization of an organisms body limits the range of frequencies for which the DWBA ray-tracing model can be applied. In general the spatial resolution of the images used in a scattering model should be fine enough that the ratio of acoustic wavelength to maximum dimension of the voxel size should be about 20:1 (Stanton and Chu, 2000). A closely related limitation is in the computational time of high resolution models. Calculating the frequency dependent, backscattering amplitude, f_{bs} , for broadband sound, where many finely incremented, discrete frequencies are considered, can take a considerably amount of computing time. Similarly, calculating f_{bs} for multiple angles of orientation, can be time intensive depending on the angular resolution. In this model calculating f_{bs} for multiple angles of orientation required significantly more processing time, per discretization, than calculations for multiple frequencies due to the rotation of the volume.

3.3.4 Application to squid

The SCT images of squid were cropped to the size of the largest cross section and then converted to binary matrices, M^l , using a simple threshold technique (Fig. 3-3). For incorporation into the DWBA ray-tracing model all voxels identified as seawater were assigned a value of “0” while voxels representing the squid’s body was assigned a value of “1”. For modeling purposes all tissue not identified as seawater was assumed to have material properties of mantle tissue. The binary conversion was insensitive to threshold level as the contrasting agent made the seawater significantly higher in x-ray attenuation than the squid’s body.

In order to model scattering by *T. pacificus*, the morphometry from the SCT

scans of *L. pealeii* was scaled so that the aspect ratio, i.e. mantle length to width ratios (L_{ml}/L_{mw}) were approximately the same. These squid are approximately 10% thicker in mantle width than *L. pealeii*. Model predictions were then compared with published data using reduced target strength [Eq. (3.4)].

3.4 Results

3.4.1 Scattering from fluid-filled, fluid spherical and finite cylindrical shells

The DWBA ray-tracing model is applied to computer generated volumes of two simple shapes, cylindrical and spherical shells. In both cases the shell and interior volume of the object are fluid materials. Reduced target strengths of spherical shells are compared with the exact modal series solution for fluid-filled, fluid spherical shells [Eq. (3.9)]. RTS predictions for cylindrical shells are compared, at normal incidence, with the modal-series-based solution for finite length, fluid-filled, fluid cylindrical shells [Eq. (3.10)] and at various orientations with the DWBA solid, finite cylinder model [Eq. (3.8)].

Shell thickness

Predictions of RTS for fluid shells of various thickness are compared with modal series results to verify that the DWBA ray-tracing model is applicable for objects containing varying degrees of inhomogeneities (Fig. 3-5 and Fig. 3-6). In both figures fractional shell thickness, τ , (see Fig. 3-1) is varied from 10% to 50% and compared with a homogeneous volume. Agreement between the DWBA ray-tracing model predictions and modal series solutions is excellent. In the spherical case (Fig. 3-5), the numerical model predictions were generally within ± 1 dB of the modal series solution for all values of shell thicknesses up to a $k_1 a$ of 12.5 and within ± 2 dB up to a $k_1 a$ of 17.5. In the cylindrical case (Fig. 3-6) the DWBA ray-tracing model matched the modal-series-based solution generally within ± 0.5 dB for $k_1 a$ up to 5 and ± 2 dB to

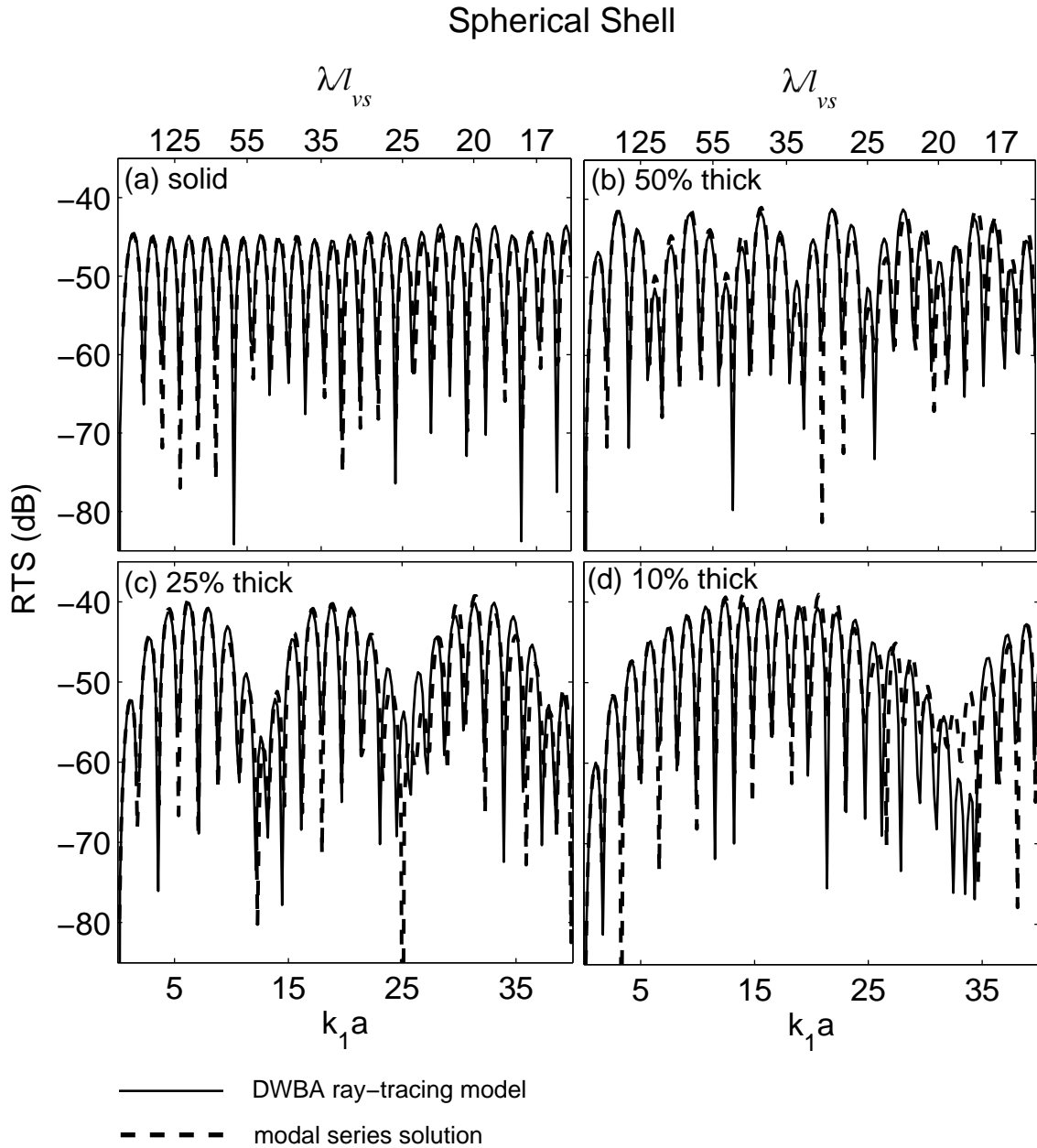


Figure 3-5: Effect of varying shell thickness on reduced target strength for a spherical, fluid-filled, fluid shell. DWBA ray-tracing predictions (solid lines) are compared with exact modal series solutions [Eq. (3.9)], (dashed lines). [Parameters: outer radius: $a = 5$ cm; material properties: $g_2 = 1.01$, $h_2 = 1.01$, $g_1 = g_3 = 1$, $h_1 = h_3 = 1$; voxel size: $l_{vs} = 0.5$ mm]

a $k_1 a$ of 12.5. In both cases some large discrepancies (> 10 dB) existed, however, these were isolated to nulls of very low RTS. As discussed in a following section, the

disagreement between the DWBA ray-tracing model and modal-series-based solutions at higher values of k_1a is a numerical issue related to voxel resolution.

Using shell thickness as a proxy for various size inhomogeneities, these results show that RTS from spherical shells and cylindrical shells at normal incidence is strongly affected by inhomogeneous material properties. Small scale structure seen here is due to interference between waves scattered from the front and back interfaces of the object. While these interference patterns, for differing shell thicknesses, are nearly identical in terms of null spacing, the large scale structure varies dramatically. An important aspect of these results is that the broadband frequency response of a weakly scattering, inhomogeneous object cannot be accurately modeled by a simple homogeneous object of the same outer form.

Material properties

It is known that the DWBA formulation is only valid for weak scatterers. In order to validate the range of accuracy for the DWBA ray-tracing model with respect to material properties, finite cylindrical shells with various sound speed and density contrasts are considered. The model predictions are compared with the modal-series-based, finite cylindrical shell solution [Eq. (3.10)] that can describe a wide range of material profiles.

Modeled RTS predictions from finite cylindrical shells with fractional shell thickness of 25% and g and h values ranging from 1.02 to 1.06 are shown in Fig. 3-7. The primary effect of increasing sound speed and density contrast was to increase the objects target strength. Frequency was varied such that the maximum k_1a of 10 equates to a minimum resolution of $\lambda/l_{vs} \simeq 25$. There is excellent agreement outside the deepest portion of the nulls (± 1 dB) up to a k_1a of 5 ($\lambda/l_{vs} \simeq 50$). Errors of up to 2 dB seen at higher k_1a is largely due to resolution issues discussed in a following section.

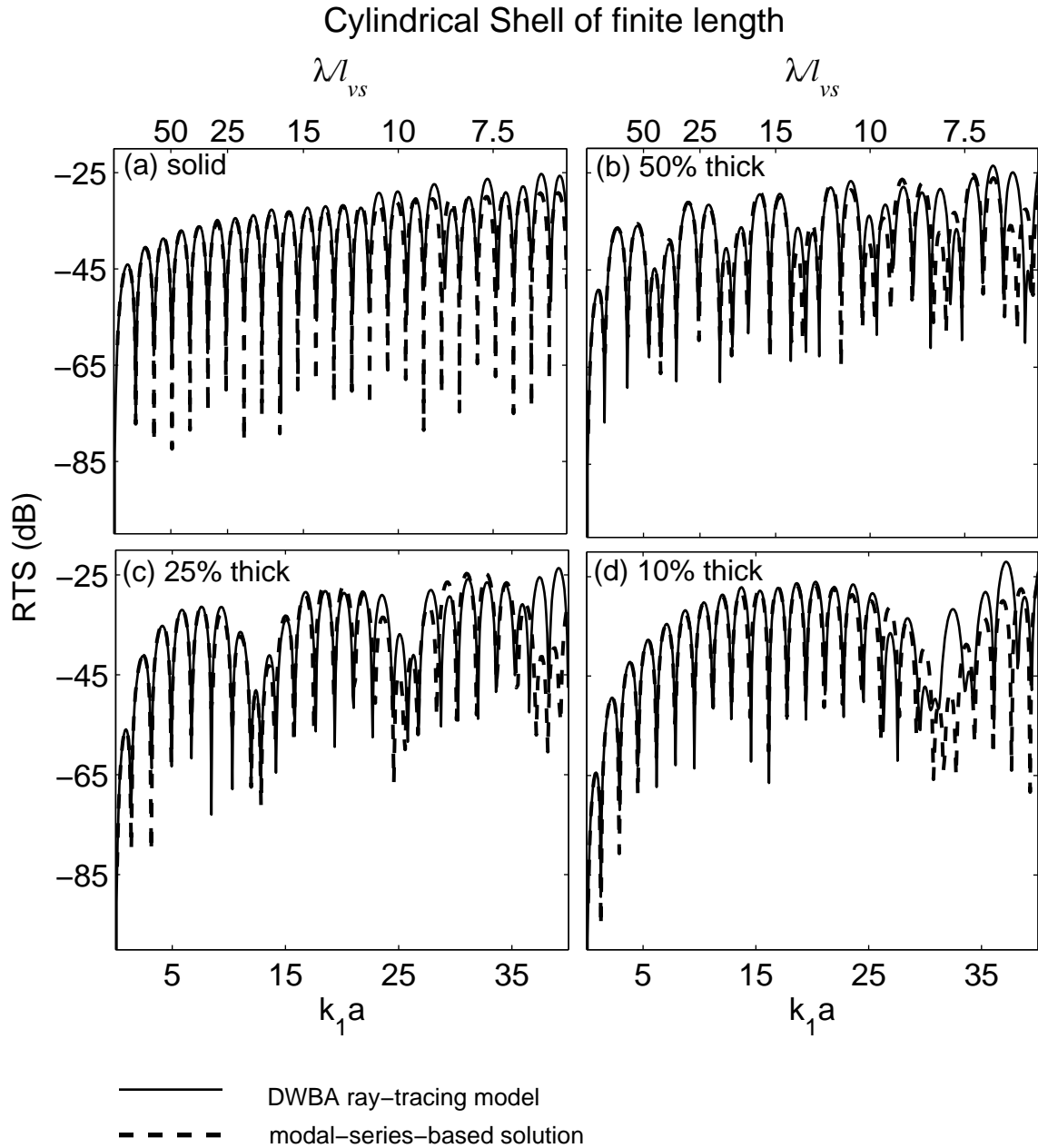


Figure 3-6: Effect of varying shell thickness on reduced target strength for a cylindrical, fluid-filled, fluid shell of finite length. DWBA ray-tracing predictions (solid lines) are compared with approximate, modal-series-based solutions, [Eq. (3.10)], (dashed lines). [Parameters: outer radius: $a = 4$ cm; aspect ratio: $a/L = 1/5$; angle of incident wave: $\theta = 0$ (normal incidence); material properties: $g_2 = 1.01$, $h_2 = 1.01$, $g_1 = g_3 = 1$, $h_1 = h_3 = 1$; voxel size: $l_{vs} = 1.0$ mm]

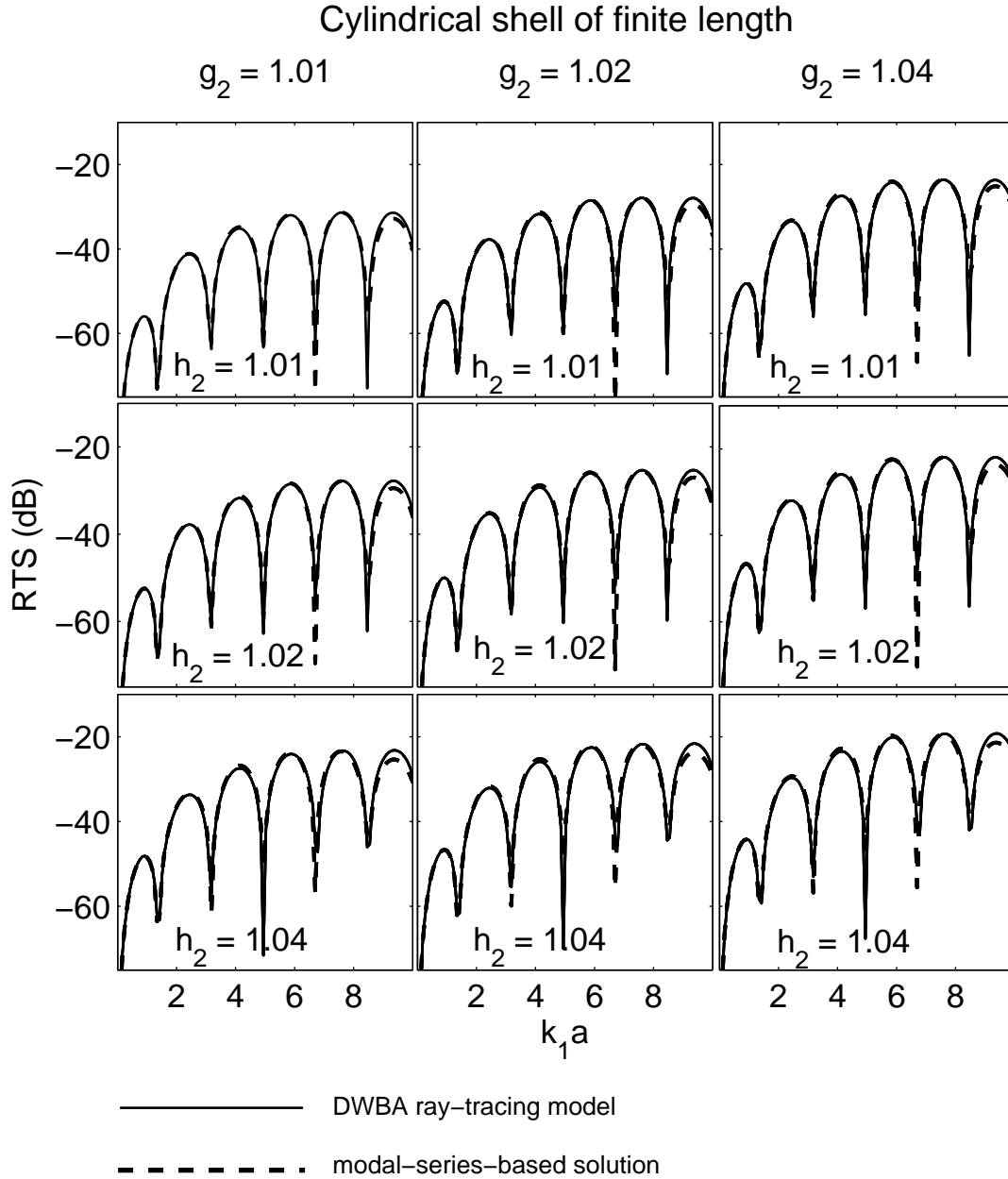


Figure 3-7: Effect of varying material properties on reduced target strength for a cylindrical, fluid-filled, fluid shell of finite length. DWBA ray-tracing predictions (solid line) are compared with approximate modal-series-based solutions for a finite cylinder, [Eq. (3.10)] (dashed lines). [Parameters: outer radius: $a = 4$ cm; fractional shell thickness: $\tau = 25\%$; aspect ratio: $a/L = 1/5$; angle of incident wave: $\theta = 0$ (normal incidence); material properties of shell: h_2 (in fig.); material properties of inner and outer fluid: $h_1 = h_3 = 1$; voxel size: $l_{vs} = 1.0$ mm]

Orientation of scattering object

In order to test the DWBA ray-tracing model for sound waves incident on an object at various angles, scattering from homogeneous cylinders at a given k_1a and varying tilt angles, θ , were considered. Since the modal-series-based solution for finite length cylinders is only accurate near broadside incidence, the ray-tracing model was compared with the DWBA solid, finite cylinder model [Eq. (3.8)], which is known to be valid for all orientations. The DWBA ray-tracing model showed very good agreement with the analytic solution (± 1 dB) except in the deepest nulls (Fig. 3-8a).

It should be noted that the values chosen for k_1a in the orientation test were neither in the deepest part of the null or at a peak in the frequency response curve (Fig. 3-6c). As seen in all the modeling tests (Figs. 3-5, 3-6, 3-7, and 3-8a) the accuracy of the DWBA ray-tracing model at very low RTS, such as in very deep nulls, is not as good as for the rest of the curve. This discrepancy, which is magnified because of the logarithmic scale, is seen in both high and low resolution models and is therefore believed to be associated with the DWBA formulation itself. It is expected that this error at low RTS is somewhat mitigated by the fact that very deep nulls are not as common in real organisms as in ideal shapes. The presence of these nulls in scattering from ideal shapes comes from nearly complete destructive interference of coherent scattering from the front and back interfaces. In real organisms the complex scattering from material property inhomogeneities and surface roughness is expected to dampen out these interference patterns.

Effects of varying voxel resolution

As the spatial resolution of a volume used to depict organism shape decreases, a numerical scattering model is susceptible to errors. This is due in large part to the inability of large voxels to accurately represent the curvature of an object. As resolution decreases, smoothly curving lines become stair-stepped facets. When these facets approach the size of the incident sound wavelength the coherent scattering from this flat face creates errors in the model solution.

Cylindrical shell of finite length

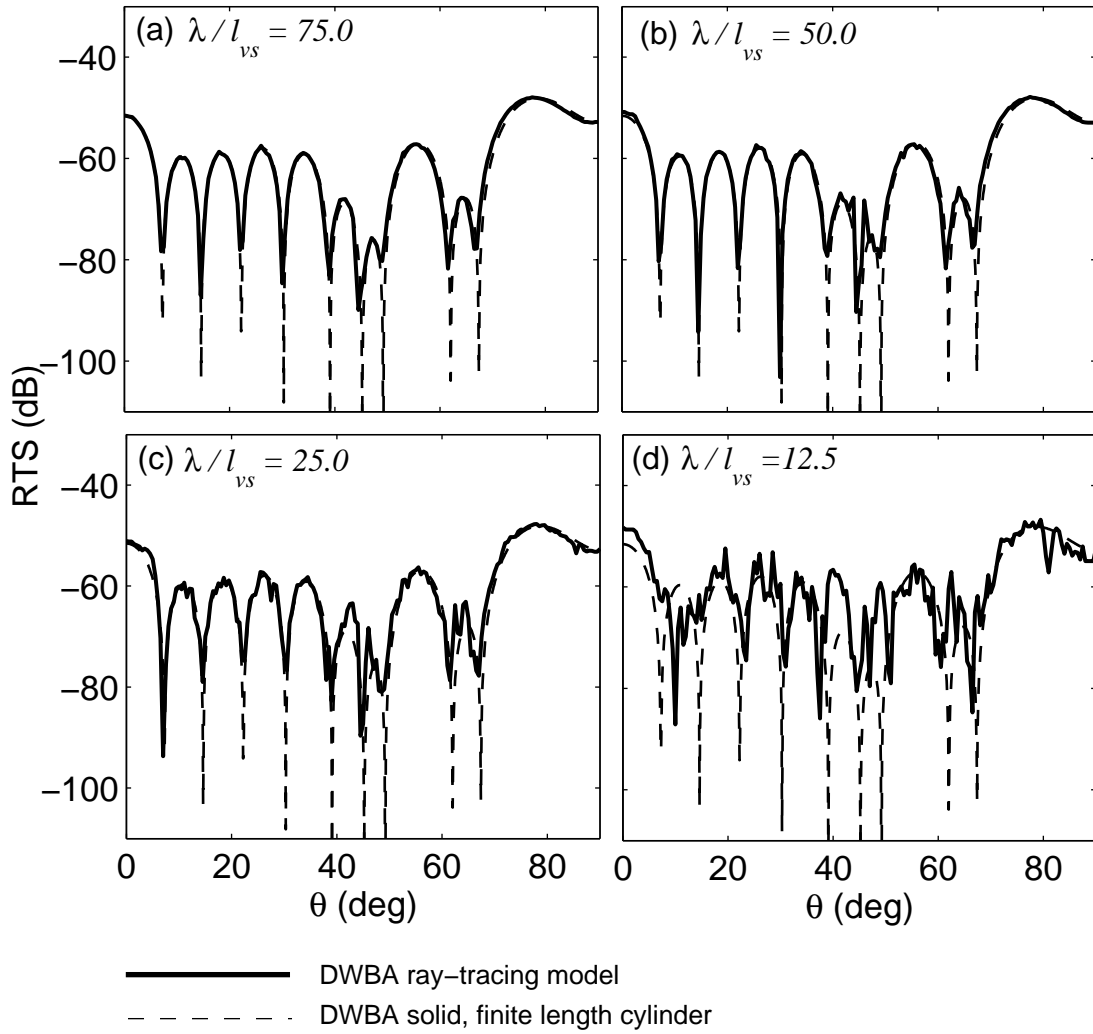


Figure 3-8: Reduced target strength versus orientation predictions for solid cylinder of finite length. DWBA ray-tracing predictions (solid line) are compared with DWBA solid, finite cylinder model, [Eq. 3.8], (dashed line). [Parameters: $g = 1.01$, $h = 1.01$, $k_1 a = 5.03$, aspect ratio, $a/L = 1/5$.]

In order to test the accuracy of the DWBA ray-tracing model at different resolutions, RTS predictions from homogeneous cylindrical volumes of the same dimensions and varying voxel size, l_{vs} , are compared to the DWBA solid, finite cylinder model [Eq. (3.8)]. Voxel size with respect to wavelength, λ/l_{vs} , is varied from 12.5 to 75 for

the RTS versus orientation curves given in Fig. 3-8. The model predictions matched the analytical solution fairly well for large scale structure at values of $\lambda/l_{vs} \geq 12.5$ and considerably better at values of $\lambda/l_{vs} \geq 25$. Small small scale structure was generally within ± 2 dB at $\lambda/l_{vs} \geq 50$.

The effects of resolution can also be seen in the results of broadside scattering from simple shapes. Figures 3-5 and 3-6 show how increasing k_1a , and thus decreasing λ/l_{vs} , affects the predictions. In the case of a spherical shell (Fig. 3-5) an accuracy of ± 2 dB requires a resolution of approximately 35. In the cylinder case a similar accuracy can be obtained by a resolution of 20. From these results it is suspected that decreased resolution has a more pronounced effect on a volume with more complex curvature (i.e. two dimensions in the spherical case as compared with one dimensional curvature in the cylindrical case). Further comparisons using spheres of increased resolution confirm that the disagreement seen at higher k_1a is due solely to resolution issues.

3.4.2 Application to squid

Reduced target strength predictions of the DWBA ray-tracing model were compared with measurements from live, freely swimming squid (Arnaya *et al.*, 1989b,c; Kang *et al.*, 2005), as well as tethered, anesthetized squid Kang *et al.* (2005). Measurements of live squid are all of the species *T. pacificus*. The model predictions use a 3-D digitization of a *L. pealeii* scaled to match the aspect ratio of a *T. pacificus*. Material properties for squid tissue and swimming tilt angle distributions come from published sources and, therefore, it should be noted that no floating parameters were necessary in these predictions.

Comparison of reduced target strength versus tilt angle with model predictions

Figure 3-9 shows reduced target strength predictions versus tilt orientation for dorsal aspect backscatter from squid. Model predictions use a 3 degree running average.

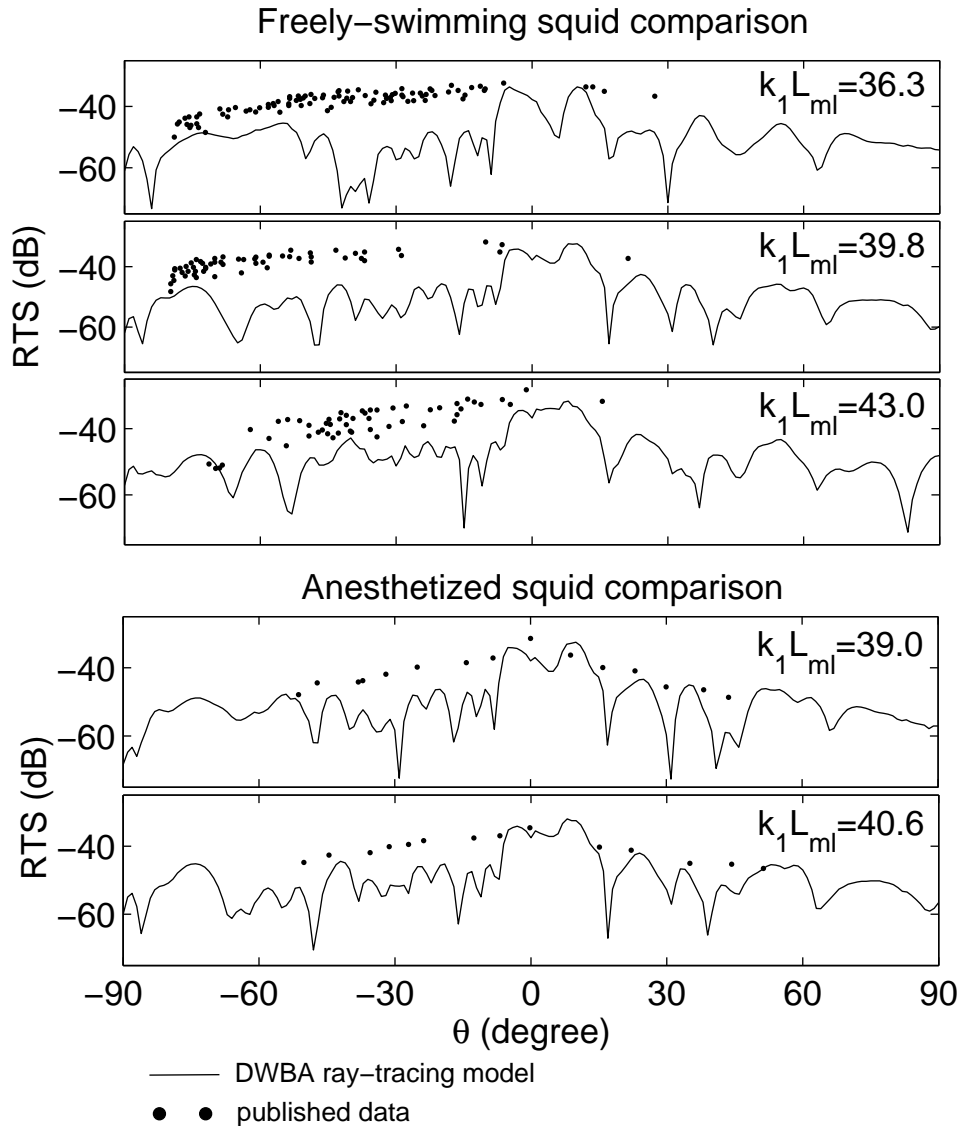


Figure 3-9: Reduced target strength versus tilt angle for squid (*T. pacificus*) using scaled morphometry of *L. pealeii*. DWBA ray-tracing model predictions (solid line) use scaled morphometry of *L. pealeii* and are compared with reduced target strengths from published measurements of *T. pacificus* (data points). Top three plots show data from live, freely swimming squid, ensonified at 38 kHz, while bottom two plots show data from anesthetized, tethered squid also ensonified at 38 kHz (Kang *et al.*, 2005).

Frequency of the incident wave, as a model parameter, was chosen that corresponds to a $k_1 L_{ml}$ that matched the frequency and mantle length of squid used in the published study. The published results of live squid ensonified at 38 kHz (Kang *et al.*, 2005) include freely swimming squid ensonified by a split beam transducer with swimming

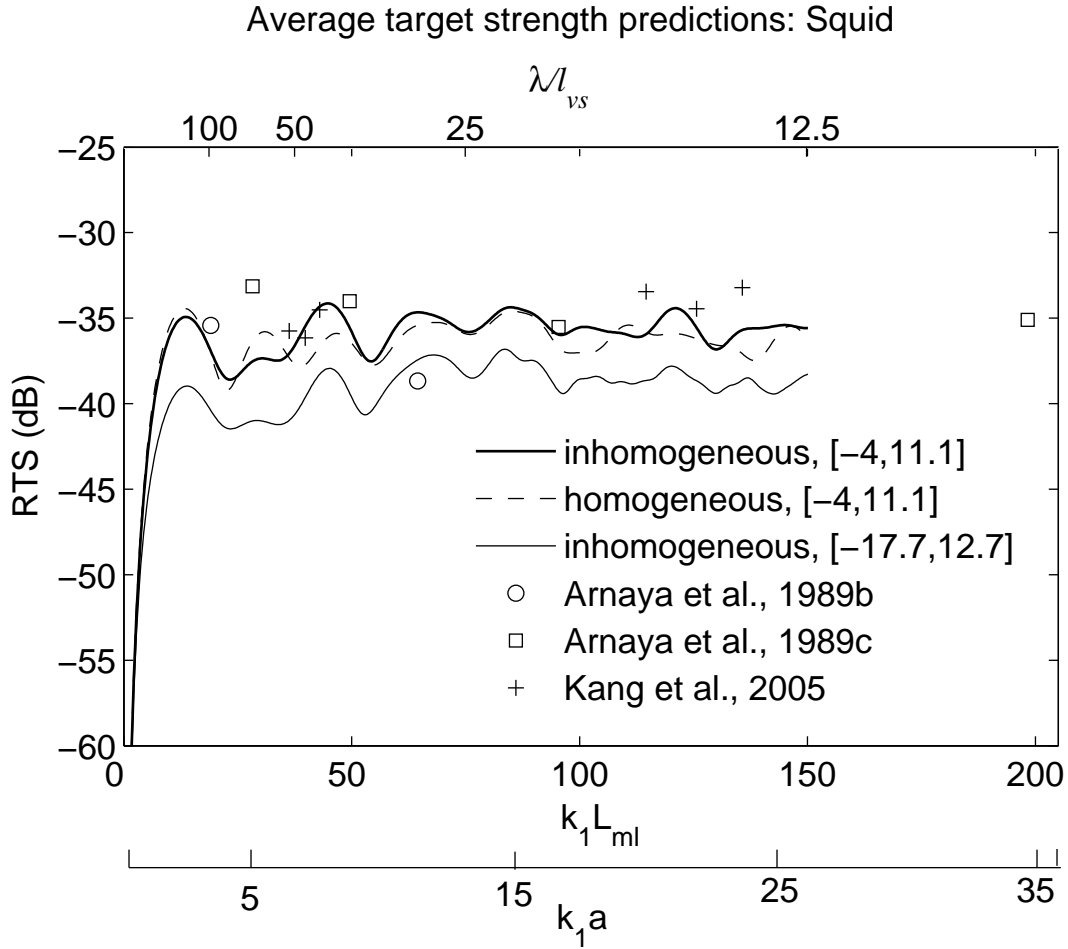


Figure 3-10: Average RTS predictions for squid (*T. pacificus*) using scaled morphometry of *L. pealeii*. DWBA ray-tracing model predictions (solid and dashed lines) are averaged over tilt angle using normal distributions limited to ± 2 standard deviations of the mean. The two tilt angle distributions presented use mean angle and standard deviation, $[\bar{\theta}, \text{s.d.}]$, from published sources of swimming squid: [-4,11.1] from Arnaya *et al.* (1989a) and [-17.7,12.7] from Kang *et al.* (2005). Predictions are compared with published results of average target strengths for live, freely swimming squid, *T. pacificus*: circles (Arnaya *et al.*, 1989b), squares (Arnaya *et al.*, 1989c), and plus signs (Kang *et al.*, 2005).

angle determined from perpendicular side-view cameras and anesthetized squid tethered at various angles of tilt. While data is sparse for the main lobe $\pm 10^\circ$, it is clear that off-broadside predictions underestimate the actual backscattered target strength by 5-10 dB or more. Furthermore, both freely swimming and tethered results show considerably less variability than predicted by the model.

Comparison of average reduced target strength with model predictions

Average RTS with respect to tilt angle is predicted for squid by compiling model realizations for two degree angle increments from -50° to $+50^\circ$. Results were weighted using two different tilt distributions of freely swimming squid from published sources (Kang *et al.*, 2005; Arnaya *et al.*, 1989a). Published measurements from three studies on target strengths of *T. pacificus* are compared with DWBA ray-tracing model predictions (Fig. 3-10). The model predictions are cut off at a $k_1 L_{\text{ml}}$ of 150 corresponding to a minimum resolution, λ/l_{vs} , of 12.5. The live measurements come from two sources. Measurements from Arnaya *et al.* (1989b,c) were estimated from mean volume backscattering target strength. The data from Kang *et al.* (2005) was measured from individual squid using a split-beam transducers at 38 and 120 kHz. The tilt distribution with a mean of -4° showed better agreement with published data.

3.5 Discussion

A scattering model that accurately treats inhomogeneities within a weakly scattering volume using a composite DWBA and ray trace formulation has been developed. This model is applicable for all frequencies and angles of scatterer orientation and can be applied to arbitrarily shaped three dimensional objects. This model is primarily limited by the spatial resolution of digital volumes used to represent shape and inhomogeneities of the scattering object. For objects with 1-D curvature, as with a cylinder, a minimum resolution of $\lambda/l_{vs} = 20$ is sufficient to model broadband, reduced target strengths at normal incidence with an accuracy of ± 2 dB. A resolution of approximately $\lambda/l_{vs} = 50$, however, is required to accurately model RTS from a cylinder over all orientations. Objects with 2-D curvature, such as a sphere, require a higher minimum resolution ($\lambda/l_{vs} = 35$) for modeling accuracy similar to the accuracy of modeling a cylinder at broadside.

The application of the DWBA ray-tracing model to simple, shelled objects shows that material property inhomogeneities have a significant impact on reduced target strength. For weakly scattering objects it is apparent that simulating an inhomoge-

neous object with a homogeneous object of the same outer form is not sufficient to accurately describe the broadband frequency response of that scatterer.

This DWBA ray-tracing model has been applied to squid using high resolution SCT scans. A result of this modeling is the discovery that, for off-broadside backscattering, something other than soft tissue and the seawater filled mantle chamber considered in this model, appears to dominate the scattering. In measurements of zooplankton, treated as a weakly scattering organism, there has been similar discrepancies between experimental measurements and DWBA predictions of scattering at off-broadside angles, or sidelobes (McGehee *et al.*, 1998; Lavery *et al.*, 2002). There are several factors that could contribute to the higher target strengths seen in measurements of these sidelobes. These factors include scattering from a complex shape, roughness of external anatomy, material properties inhomogeneities, flexing or bending of the animal, and phase variability from the influence of noise (Stanton *et al.*, 1998a; Demer and Conti, 2003; Amakasu and Furusawa, 2006). Stanton and Chu (2000) showed that for zooplankton, axial variations in material properties, simulating internal inhomogeneities in zooplankton, had the effect of generally raising the sidelobe levels. For squid, swimming motion has also been shown to be a factor in scattering (Arnaya and Sano, 1990a).

In this study the comparison of predictions versus measured reduced target strengths of both tethered, anesthetized squid and freely swimming squid show sidelobe discrepancies. Therefore, although swimming motion and changes in body shape cannot be ruled out as a contributing factor, other factors most likely apply. Considering the incorporation of both the complex outer shape of squid and the interior morphology of the mantle chamber used in this model, only a few possible factors remain. One probable factor is inhomogeneities in the internal anatomy of the squid. The interior body of the squid includes a long thin pen, a parrot-like beak, statoliths (small, bony inner ear organs), a hard cartilaginous cranium, and hard lenses in the eye (Williams, 1909). Iida *et al.* (2006), also identifies the liver, a low density organ surrounded by higher density tissue, as a likely scatterer of sound. In combination it seems likely that scattering from the variety of inhomogeneities within a squid's

body could significantly contribute to scattering and even dominate the scattering from off-broadside orientations. It is suggested that future work on scattering from squid include focused array transducer measurements along the length of a live squid. This type of measurement can localize and quantify relative scattering contributions from different areas of an organism's body (Nash *et al.*, 1987).

Orientation averaged, reduced target strength results show better agreement between modeling predictions and published data. This is likely due to the fact that broadside and near-broadside echoes dominate the averages in the given tilt distributions. Scattering from organisms at broadside angles are less sensitive to shape and material profile because the scattering is dominated by echoes from the front and back interfaces (Stanton *et al.*, 1993; Stanton and Chu, 2000). Errors in the predictions due to inhomogeneities not included in this model are, thus, less significant when averages include the broadside scattering levels. In general, this model produces reasonable predictions for squid and may have direct application to other soft bodied marine organisms.

Chapter 4

Summary and conclusion

This thesis investigates the scattering of broadband echolocation signals emitted by beaked whales. For the first time, echoes, recorded *in situ* from prey of echolocating toothed whales, have been comprehensively examined. Furthermore an advance to an existing scattering model has been motivated by this analysis to give further insight into the scattering by prey. The following paragraphs summarize the research presented here, present recommendations for future work, and list the contributions of this thesis.

4.1 Scattering of echolocation signals

New methods and technologies in data collection often lead to exciting research opportunities. Recordings of beaked whale hunting signals and the resultant, backscattered echoes have provided a new insight into the relationship between these predators and their prey. Scattering research, which has developed over the years as a means of surveying marine populations and fisheries stocks, can now be applied to help understand a complex predator behavior. The research detailed in this thesis shows that data acquired in this form can be studied to determine how and if beaked whales acoustically discriminate their prey from other scatterers in their environment. While no clear answer is determined, as to what specific feature or features within the frequency response of their prey is key to the classification process, it does appear that

there is an acoustic basis, beyond target strength, for this discrimination. Specifically, the spectral structure content, i.e. patterns of peaks and nulls in the echoes' spectra, appear to play an important role in the whale's selection of prey.

4.2 Modeling

The goal of modeling acoustic scattering is to both increase the understanding of the scattering process from complex objects, such as marine organisms, as well as provide a useful tool in analyzing *in-situ* acoustic data from marine populations. Generalizing existing models can help extend their application to organisms of greater complexity. The application of the DWBA model to inhomogeneous bodies broadens the applicability of this model and improves accuracy for such objects. It is believed that this high resolution, DWBA ray-tracing model has a useful application to squid with some reservations, in its current form, for predictions of off-broadside scattering. This limitation will need to be addressed if discrete scattering predictions are going to be useful in individual echo classification schemes for squid. Nonetheless, the results from this modeling work, qualitatively, provide insight into the whale echolocation problem. Additionally, it is expected that this model will have direct application to other complex, soft-bodied organisms.

4.3 Recommendations for future work

One of the limitations of this study is the small amount of data available. Useful acoustic data of discrete echoes from prey of an echolocating whale is limited to well-placed tags in which the target echoes are not shadowed by the whale's body. It is hoped that future measurements from tagged whales will provide more data that can be used to further analyze both the whale's behavior and also help characterize the prey field where these animals hunt.

It is suspected that future development of automated algorithms is possible to classify series of echoes, such as the prey echo trains discussed in this paper, into

broad morphological categories based on target strengths and spectral structure of the echoes. Requirements for this type of work include high quality *in situ* data like that analyzed here, accurate and frequency-specific source levels for the species of whale being studied, and expected prey based on stomach content data of similar species of whales foraging in the same habitat. Scattering models used in such algorithms depend on accurate morphological features, size, and material properties of expected prey. Although unambiguous classification of species may not be possible, broad categories such as swimbladder bearing fish, non-swimbladder-bearing fish, squid, etc. may be feasible.

4.4 Contributions of this thesis

- Analysis of echo characteristics from prey of an echolocating beaked whale. Comparison with non-whale-selected scatterers gives evidence of an acoustic basis for prey selection by the Blainville's beaked whale.
- Application of the distorted wave Born approximation (DWBA) to fully 3-D inhomogeneous, weakly-scattering objects using a combined volume integration and ray trace approach.
- Application of DWBA ray-tracing model to squid using high resolution spiral computerized tomography (SCT) scans for internal and external morphology. This advancement serves dual purposes: (1) to accurately model acoustic scattering from a marine organisms, (2) to add further insight into the echolocation behavior of beaked whales.

Appendix A

Modal series coefficients for fluid-filled shells

As explained in the theory section of this article, the ray-tracing DWBA model developed in this work is validated, in part, by comparison to exact modal series solutions for fluid-filled, fluid spherical shells and modal-series-based solutions for finite cylindrical shells. The modal series solutions are derived by separating the wave equation in spherical and cylindrical coordinate systems, respectively, and applying two boundary conditions at each interface: continuity of pressure and continuity of radial velocity. The resulting modal series solution coefficients for spherical shells and infinite length cylindrical shells are presented here. In the examples given in this this paper, the properties of the fluid surrounding the scatterer are denoted by the subscript “1”, the fluid shell of the scatterer is denoted by subscript “2”, and the fluid inside the shell is denoted by the subscript “3” (Fig. 3-1).

A.0.1 Spherical shells

The modal series coefficients for a fluid-filled, fluid spherical shell expressed as the variable, A_n , in Eq. (3.9) is given below as the determinants of two matrices. These matrices contain the spherical bessel functions of the first kind, j_n , the second kind η_n , and the third kind (also known as the spherical Hankel function of the first kind,

$h_n^{(1)}$). Primes on the Bessel functions, (e.g. $h_n^{(1)'}(k_1a)$), indicate derivatives with respect to their argument.

$$A_n = \frac{\begin{vmatrix} j_n(k_1a) & 0 & -j_n(k_2a) & -\eta_n(k_2a) \\ j_n'(k_1a) & 0 & -\frac{\rho_1 c_1}{\rho_2 c_2} j_n'(k_2a) & -\frac{\rho_1 c_1}{\rho_2 c_2} \eta_n'(k_2a) \\ 0 & -j_n(k_3b) & j_n(k_2b) & \eta_n(k_2b) \\ 0 & -\frac{\rho_2 c_2}{\rho_3 c_3} j_n'(k_3b) & j_n'(k_2b) & \eta_n'(k_2b) \end{vmatrix}}{\begin{vmatrix} h_n^{(1)}(k_1a) & 0 & -j_n(k_2a) & -\eta_n(k_2a) \\ h_n^{(1)'}(k_1a) & 0 & -\frac{\rho_1 c_1}{\rho_2 c_2} j_n'(k_2a) & -\frac{\rho_1 c_1}{\rho_2 c_2} \eta_n'(k_2a) \\ 0 & -j_n(k_3b) & j_n(k_2b) & \eta_n(k_2b) \\ 0 & -\frac{\rho_2 c_2}{\rho_3 c_3} j_n'(k_3b) & j_n'(k_2b) & \eta_n'(k_2b) \end{vmatrix}} \quad (\text{A.1})$$

A.0.2 Cylindrical shells

The modal series coefficients for a fluid-filled, fluid infinite cylindrical shell, expressed as the variable, B_n , in Eq. (3.10), is given below as the determinants of two matrices. These matrices contain the cylindrical bessel functions of the first kind, J_n , the second kind (also known as the Neumann function, N_n) and the third kind (also known as the Hankel function of the first kind, $H_n^{(1)}$). Primes on the Bessel functions, (e.g. $H_n^{(1)'}(k_1a)$), indicate derivatives with respect to their argument.

$$B_n = \frac{\begin{vmatrix} J_n(k_1a) & 0 & -J_n(k_2a) & -N_n(k_2a) \\ J_n'(k_1a) & -\frac{\rho_1 c_1}{\rho_2 c_2} J_n'(k_2a) & -\frac{\rho_1 c_1}{\rho_2 c_2} N_n'(k_2a) & \\ 0 & -J_n(k_3b) & J_n(k_2b) & N_n(k_2b) \\ 0 & -\frac{\rho_2 c_2}{\rho_3 c_3} J_n'(k_3b) & J_n'(k_2b) & N_n'(k_2b) \end{vmatrix}}{\begin{vmatrix} H_n^{(1)}(k_1a) & 0 & -J_n(k_2a) & -N_n(k_2a) \\ H_n^{(1)'}(k_1a) & -\frac{\rho_1 c_1}{\rho_2 c_2} J_n'(k_2a) & -\frac{\rho_1 c_1}{\rho_2 c_2} N_n'(k_2a) & \\ 0 & -J_n(k_3b) & J_n(k_2b) & N_n(k_2b) \\ 0 & -\frac{\rho_2 c_2}{\rho_3 c_3} J_n'(k_3b) & J_n'(k_2b) & N_n'(k_2b) \end{vmatrix}} \quad (\text{A.2})$$

Appendix B

Algorithms for DWBA ray-tracing model

The algorithm used to calculate backscattering amplitude, f_{bs} , for inhomogeneous objects consists of two files, given in this section, that are written for MATLAB technical computing software (ver. 7.2.0.232). This example uses three material properties but the algorithms can be easily modified to accept any number of discrete material properties. The first file, “DWBA_3D_ray.m”, is an algorithm that calculates the amplitude and phase for each volume element and numerically integrates these results for each frequency discretization of a broadband frequency array. This file calls on the second algorithm “vrotate.m” that rotates the volume so that the incident wavenumber vector \vec{k}_i is orthogonal to the matrices of size $[r,c]$ in the 3-D volume matrix, \tilde{S}_v , of size $[r,c,im]$.

```

%%%%%%%%%%%%%%%%%%%%%%%%%%%%%%%%%%%%%%%%%%%%%%%%%%%%%%%%%%%%%%%%%%%%%%%%
%%DWBA_3D_ray.m                                                    %%
%%Ben Jones    4/11/06                                           %%
%%%%%%%%%%%%%%%%%%%%%%%%%%%%%%%%%%%%%%%%%%%%%%%%%%%%%%%%%%%%%%%%%%%%%%%%
% Computes volume integral DWBA of scattering
% with multiple material properties
% uses ray tracing to track phase
% uses CT scan images for high resolution morphometry
clear, close all

%%                USER SELECTED VARIABLES
vol_file = 'LP05' ; %scattering volume filename
%incident wave
phi = 0 ;          %0/180 dorsal/ventral, 90/-90=lft/rt lateral
theta = 45 ;      %tilt: (-) head down , (+) head up
fmin = 1e-30 ;    %min frequency
fmax = 100e3 ;    %max frequency
df = 0.5e3 ;      %[Hz] frequency resolution
%set material properties
rho0 = 1020 ; %[kg/m^3] (medium tagged with '0') %1020 for squid
c0 = 1500 ;  %[m/s]
g1 = 1.043 ; %rho1/rho0 (medium tagged with '1') %1.043 for squid
h1 = 1.053 ; %c1/c0                                     %1.053 for squid
g2 = 1.0 ; %rho2/rho0 (medium tagged with '2')
h2 = 1.0 ; %c2/c0
%scan resolution
ps = 5e-4 ;  % [m] voxel size **assumes cubic voxels

```

```

%%                                DIRECTORIES
HOME_DIR = pwd ;
DATA_DIR = [HOME_DIR, '\data'] ;
VOL_DIR = [HOME_DIR, '\volumes'] ;

%%                                ROTATE VOLUME (orthogonalize K vector)
[BWtop] = vrotate(phi,theta,VOL_DIR,vol_file,0) ;
    cd(VOL_DIR)
    save('BWtop','BWtop') %saves rotated volume in volume directory
    cd(HOME_DIR)
fprintf('volume rotated successfully')

%%                                LOOP PARAMETERS
[r,c,im] = size(BWtop) ;
%frequency array
farray = fmin:df:fmax ; flen = length(farray) ;
%preallocate memory
fbs_dwba = zeros(1,flen) ; f_dwba = zeros(1,flen) ;

%%                                FREQUENCY LOOP
for fnx = 1:flen f = farray(fnx) theta
%preallocate memory
dph = zeros(r,c,im) ; dA = zeros(r,c,im) ;

%wavenumbers in various mediums
k(1) = 2*pi*f/c0 ;      %[rad/m] wavenumber in medium '0'
k(2) = k(1)/h1 ;      %[rad/m] wavenumber in medium '1'
k(3) = k(1)/h2 ;      %[rad/m] wavenumber in medium '2'

```

```

%DWBA coefficients
%amplitude in medium '1'
Cb_1 = 1/(g1*h1^2)+1/g1-2 ;          %gamma_kappa - gamma_rho
Ca_1 = k(1).*k(1)*Cb_1/(4*pi) ;     %summation coefficient
%amplitude in medium '2'
Cb_2 = 1/(g2*h2^2)+1/g2-2 ;
Ca_2 = k(1).*k(1)*Cb_2/(4*pi) ;

%find differential phase for each voxel
dx = ps ; dy = ps ; dz = ps ;
fldnx0 = find(BWtop==0) ; %for medium (tag = '0')
dph(fldnx0) = (k(1)*dx) ;
fldnx1 = find(BWtop==1) ; %for medium (tag = '1')
dph(fldnx1) = (k(2)*dx) ;
fldnx2 = find(BWtop==2) ; %for medium (tag = '2')
dph(fldnx2) = (k(3)*dx) ;
%1-way phase to center of voxel
phase = cumsum(dph,3)-dph/2 ; %cumulative summation of phase

%find differential amplitudes for each voxel
dv = dx.*dy.*dz ;
dA(fldnx1) = Ca_1*exp(2*i*phase(fldnx1))*dv ;
dA(fldnx2) = Ca_2*exp(2*i*phase(fldnx2))*dv ;

%volume summation
fbs_dwba(fnx) = sum(sum(sum(dA))) ;
f_dwba(fnx) = f ;

clear dph phase fldnx0 fldnx1 fldnx2 dA
end

```

```

%%                                COMPILE AND SAVE DATA

%calculate target strength
sigmabs = (abs(fbs_dwba)).^2 ; TS_dwba = 10*log10(sigmabs) ;

%parameters
param.c0 = c0 ; param.c1 = h1*c0 ; param.c2 = h2*c0 ;
param.rho0 = rho0 ; param.rho1 = g1*rho0 ; param.rho2 = g2*rho0 ;
param.phi = phi ; param.theta = theta ;
param.ps = ps ;

data_file = [vol_file,'_',num2str(phi),'_',num2str(theta)] ;
Q = input('Do you want to save these results?','s') ;
if Q == 'y'
    cd(DATA_DIR)
    save(data_file,'fbs_dwba','TS_dwba','f_dwba','param')
    cd(HOME_DIR)
end

```

```

function [BWtop] = vrotate(phi,theta,voldir,file,sav)
%%%%%%%%%%%%%%%%%%%%%%%%%%%%%%%%%%%%%%%%%%%%%%%%%%%%%%%%%%%%%%%%%%%%%%%%
%%volume_rotate                                     %%
%%Ben Jones 3/21/06                                 %%
%%%%%%%%%%%%%%%%%%%%%%%%%%%%%%%%%%%%%%%%%%%%%%%%%%%%%%%%%%%%%%%%%%%%%%%%
% rotates to selected coordinate system
%
% phi: rotate about center column of center frame
% theta: rotate about center row of center frame
% **note: setting phi,theta = 0 rotates cross-
% section slices to longitudinal slices
% voldir: volume directory
% file: volume file
% sav: 1/0 (1=query to save / 0=don't save)

%%                                DIRECTORIES
HOME_DIR = pwd ;

%%                                LOAD VOLUME
cd(voldir)
load(file) ;
cd(HOME_DIR)

[r,c,list1] = size(BWtop) ; %BWtop is 3-D volume matrix prev. loaded
BW = BWtop ;

%%                                ROTATE IN PHI DIRECTION
BWph1 = imrotate(BW(:,:,1),phi,'nearest','loose') ;
[sz1,sz2] = size(BWph1) ;
BWph1 = zeros(sz1,sz2,list1) ;
for nx = 1:list1 %for each original image

```

```

    %nx
    BWphi(:,:,nx) = imrotate(BW(:,:,nx),phi,'nearest','loose') ;
end

%%          ROTATE IN THETA DIRECTION
%first reslice along longitudinal axes and pasting as array
[r,c,p] = size(BWphi) ;
BWside = zeros(r,p,c) ;
for nim = 1:c %for each new image (= number of cols of old images)
    %nim
    for oim = 1:p %for each new image column (old image slice)
        BWside(:,oim,nim) = BWphi(:,c-nim+1,oim) ; %from right to left
    end
end
end
%rotate
BWth1 = imrotate(BWside(:,:,1),theta,'nearest','loose') ;
[sz1,sz2] = size(BWth1) ;
BWtheta = zeros(sz1,sz2,c) ;
for phnx = 1:c %for each new image (= number of cols of old images)
    %phnx
    BWtheta(:,:,phnx) = imrotate(BWside(:,:,phnx),theta,'nearest','loose') ;
end
end

%%          RESLICE IN ORTHOGONAL PLANES
%reslice matrix from top to bottom
[r,c,p] = size(BWtheta) ;
BWtop = zeros(p,c,r) ;
for nim = 1:r %for each new image (= number of rows of old images)
    %nim
    for oim = 1:p %for each new image row (old image slice)

```

```

        BWtop(p-oim+1,:,nim) = BWtheta(nim,:,oim) ; %from right to left
    end
end

%%                SAVE DATA
if sav == 1
    Q=input('Do you want to save the parameters? ','s') ;
    if Q == 'y'
        filename = [file,'_',num2str(phi),'_',num2str(theta)] ;
        cd(voldir)
        save(filename,'BWtop')
        cd(HOME_DIR)
    end
end
end

```


Bibliography

- Akamatsu, T., Wang, D., Wang, K., and Naito, Y. (2005). “Biosonar behavior of free-ranging porpoises”, *Proc R Soc Biol Sci Ser B* **272**, 797–801.
- Amakasu, K. and Furusawa, M. (2006). “The target strength of Antarctic krill (*Euphausia superba*) measured by the split-beam method in a small tank at 70 kHz”, *ICES J Mar Sci* **63**, 36–45.
- Anderson, V. C. (1950). “Sound scattering from a fluid sphere”, *J Acoust Soc Am* **22**, 426–431.
- Arnaya, I. N. and Sano, N. (1990a). “Studies on acoustic target strength of squid. 5. effect of swimming on target strength of squid”, *Bull. Fac. Fish. Hokkaido Univ.* **41**, 18–31.
- Arnaya, I. N. and Sano, N. (1990b). “Studies on acoustic target strength of squid. 6. simulation of squid target strength by prolate spheroidal model”, *Bull. Fac. Fish. Hokkaido Univ.* **41**, 32–42.
- Arnaya, I. N., Sano, N., and Iida, K. (1989a). “Studies on acoustic target strength of squid. 2. effect of behaviour on averaged dorsal aspect target strength”, *Bull. Fac. Fish. Hokkaido Univ.* **40**, 83–99.
- Arnaya, I. N., Sano, N., and Iida, K. (1989b). “Studies on acoustic target strength of squid. 3. measurement of the mean target strength of small live squid”, *Bull. Fac. Fish. Hokkaido Univ.* **40**, 100–115.

- Arnaya, I. N., Sano, N., and Iida, K. (1989c). “Studies on acoustic target strength of squid 4. measurement of the mean target strength of relatively large-sized live squid”, *Bull. Fac. Fish. Hokkaido Univ.* **40**, 169–181.
- Au, W. W. L. (1993). *The Sonar of Dolphins* (Springer-Verlag, New York).
- Au, W. W. L., Ford, J. K. B., Horne, J. K., and Allman, K. A. N. (2004). “Echolocation signals of free-ranging killer whales (*Orcinus orca*) and modeling of foraging for chinook salmon (*Oncorhynchus tshawytscha*)”, *J Acoust Soc Am* **115**, 901–909.
- Au, W. W. L., Kastelein, R. A., Rippe, T., and Schooneman, N. M. (1999). “Transmission beam pattern and echolocation signals of a harbor porpoise (*Phocoena phocoena*)”, *J Acoust Soc Am* **106**, 3699–3705.
- Au, W. W. L. and Pawloski, J. L. (1989). “Detection of noise with rippled spectra by the Atlantic bottlenose dolphin”, *J Acoust Soc Am* **86**, 591–596.
- Chu, D. Z., Foote, K. G., and Stanton, T. K. (1993). “Further analysis of target strength measurements of Antarctic krill at 38 and 120 kHz - comparison with deformed cylinder model and inference of orientation distribution”, *J Acoust Soc Am* **93**, 2985–2988.
- Chu, D. Z., Wiebe, P., and Copley, N. (2000). “Inference of material properties of zooplankton from acoustic and resistivity measurements”, *ICES J Mar Sci* **57**, 1128–1142.
- Demer, D. A. and Conti, S. G. (2003). “Validation of the stochastic distorted-wave Born approximation model with broad bandwidth total target strength measurements of Antarctic krill”, *ICES J Mar Sci* **60**, 625–635.
- Dubrovskiy, N. (1989). “On the two auditory subsystems in dolphins: Sensory Abilities of Cetaceans”, in *Proceedings of a NATO Advanced Workshop and Symposium of the Fifth International Theriological Congress on Sensory Abilities of Cetaceans*, edited by R. Thomas, J.A.; Kastelein, NATO ASI Series, 233–254 (Plenum Press, 1990, Rome).

- Foote, K. G. (1997). “Target strength of fish”, in *Encyclopedia of Acoustics*, edited by M. J. Crocker, 493–500 (John Wiley & Sons, Inc.).
- Foote, K. G. and Stanton, T. K. (2000). “Acoustical methods”, in *ICES Zooplankton Methodology Manual*, edited by R. Harris, P. Wiebe, J. Lenz, H. R. Skjoldal, and M. Huntley, 223–258 (Academic Press, San Diego).
- Fuzessery, Z., Feng, A., and Supin, A. (2004). “Central auditory processing of temporal information in bats and dolphins”, in *Echolocation in Bats and Dolphins*, edited by C. F. V. M. Thomas, J.A.; Moss, 115–122 (University of Chicago Press, Chicago).
- Galambos, R. (1942). “The avoidance of obstacles by flying bats: Spallanzani’s ideas (1794) and later theories.”, *Isis* **34**, 132–140.
- Goss, C., Middleton, D., and Rodhouse, P. (2001). “Investigations of squid stocks using acoustic survey methods”, *Fish. Res.* **54**, 111–121.
- Griffin, D. R. (1944). “Echolocation by blind men, bats and radar”, *Science* **100**, 589–590.
- Griffin, D. R. (1953). “Bat sounds under natural conditions with evidence for the echolocation of insect prey”, *J Exp Biol* **123**, 435–466.
- Hashimoto, T. and Maniwa, Y. (1952, in Japanese). “Studies on fish finder. 3. Studies on sound speed in fish body.”, *Tech. Rep. Fish. Boat* **3**, 208–215.
- Hofer, M., ed. (2000). *CT Teaching Manual* (Thieme, New York).
- Horne, J. K. (2000). “Acoustic approaches to remote species identification: a review”, *Fish. Oceanogr.* **9**, 356–371.
- Iida, K., Takahashi, R., Tang, Y., Mukai, T., and Sato, M. (2006). “Observation of marine animals using underwater acoustic camera”, *Jpn. J. Appl. Phys.* **45**, 4875–4881.

- Johnson, M., Madsen, P., Zimmer, W., Aquilar-Soto, N., and Tyack, P. (**submitted**). “Bi-modal click production in Blainsville’s beaked whales (*Mesoplodon densirostris*) echolocating for food” .
- Johnson, M., Madsen, P. T., Zimmer, W. M. X., de Soto, N. A., and Tyack, P. L. (**2004**). “Beaked whales echolocate on prey”, *Proc. R. Soc. Lond. B* **271**, S383–S386.
- Johnson, M. P. and Tyack, P. L. (**2003**). “A digital acoustic recording tag for measuring the response of wild marine mammals to sound”, *IEEE J. Ocean . Eng.* 3–12.
- Johnson, R. (**1977**). “Sound scattering from a fluid sphere revisited”, *J Acoust Soc Am* **61**, 375–377.
- Jones, B. A., Lavery, A. C., and Stanton, T. K. (**in prep.a**). “Acoustic scattering by weakly scattering shelled objects: Application to squid”, *J Acoust Soc Am* .
- Jones, B. A., Stanton, T. K., Lavery, A. C., Johnson, M. P., Madsen, P. T., and Tyack, P. L. (**in prep.b**). “Classification of broadband echoes from prey of a foraging Blainville’s beaked whale”, *J Acoust Soc Am* .
- Kang, D. Y., Iida, K., Mukai, T., and Hwang, D. (**2004**). “Acoustic target strength of Japanese common squid, *Todarodes pacificus*, and important parameters influencing its ts: swimming angle and material properties”, in *OCEANS’04 MTS/IEEE/TECHNO-OCEAN’04*, 364–369 (Kobe).
- Kang, D. Y., Mukai, T., Iida, K., Hwang, D. J., and Myoung, J. G. (**2005**). “The influence of tilt angle on the acoustic target strength of the Japanese common squid (*todarodes pacificus*)”, *ICES J Mar Sci* **62**, 779–789.
- Lavery, A. C., Stanton, T. K., McGehee, D. E., and Chu, D. (**2002**). “Three-dimensional modeling of acoustic backscattering from fluid-like zooplankton”, *J Acoust Soc Am* **111**, 1197–1210.

- Lawson, G. L., Wiebe, P. H., Ashjian, C. J., Gallager, S. M., Davis, C. S., and Warren, J. D. (2004). “Acoustically-inferred zooplankton distribution in relation to hydrography west of the Antarctic peninsula”, *Deep-Sea Res. Pt. II* **51**, 2041–2072.
- MacLennan, D. N. and Simmonds, E. J. (1992). *Fisheries Acoustics* (Chapman & Hall, London).
- Madsen, P. T., Johnson, M., de soto, N., Zimmer, W. M. X., and Tyack, P. (2005). “Biosonar performance of foraging beaked whales (*Mesoplodon densirostris*)”, *J Exp Biol* **208**, 181–194.
- Martin, L. V., Stanton, T. K., Wiebe, P. H., and Lynch, J. F. (1996). “Acoustic classification of zooplankton”, *ICES J Mar Sci* **53**, 217–224.
- McGehee, D. E., O’Driscoll, R. L., and Traykovski, L. V. M. (1998). “Effects of orientation on acoustic scattering from Antarctic krill at 120 kHz”, *Deep-Sea Res. Pt. II* **45**, 1273–1294.
- Mead, J. G. (1989). “Beaked whales of the genus *Mesoplodon*”, in *Handbook of marine mammals*, edited by S. H. Ridgway and R. J. Harrison, volume 4, 349–430 (Academic Press, London ; New York).
- Morse, P. M. and Ingard, K. U. (1968). *Theoretical Acoustics* (McGraw-Hill, New York,).
- Mukai, T., Iida, K., Sakaguchi, K., and Abe, K. (2000). “Estimations of squid target strength using a small cage and theoretical scattering models”, *Proc. JSPS-DGHE Int. Symp.* **10**, 135–140.
- Nachtigall, P. E. (1980). “Odontocete echolocation performance on object size, shape, and material: Animal Sonar Systems”, in *Proceedings of the Second International Interdisciplinary Symposium on Animal Sonar Systems*, edited by J. Busnel, R.G.;Fish, 71–95 (Plenum Press, Jersey, Channel Islands).

- Nash, D. M., Sun, Y., and Clay, C. S. (1987). “High resolution acoustic structure of fish”, *J. Cons. int. Explor. Mer.* **43**, 23–31.
- Pauly, D., Trites, A. W., Capuli, E., and Christensen, V. (1998). “Diet composition and trophic levels of marine mammals”, *ICES J Mar Sci* **55**, 467–481.
- Pierce, G. and Griffin, D. (1938). “Experimental determination of supersonic notes emitted by bats”, *J Mammal* **19**, 454–455.
- Reeder, D. B., Jech, J. M., and Stanton, T. K. (2004). “Broadband acoustic backscatter and high-resolution morphology of fish: Measurement and modeling”, *J Acoust Soc Am* **116**, 747–761.
- Roper, C., Sweeney, M., and Nauen, C. (1984). *Cephalopods of the world. An annotated and illustrated catalogue of species of interest to fisheries.*, volume 3 of *FAO Species Catalogue* (FAO, Rome).
- Sakurai, Y., Kiyofuji, H., Saitoh, S., Goto, T., and Hiyama, Y. (2000). “Changes in inferred spawning areas of *Todarodes pacificus* (Cephalopoda: Ommastrephidae) due to changing environmental conditions”, *ICES J Mar Sci* **57**, 24–30.
- Schmidt, S. (1992). “Perception of structured phantom targets in the echolocating bat, *Megaderma lyra*”, *J Acoust Soc Am* **91**, 2203–2223.
- Siemers, B. M. and Schnitzler, H. U. (2000). “Natterer’s bat (*Myotis nattereri*, Kuhl, 1818) hawks for prey close to vegetation using echolocation signals of very broad bandwidth”, *Behav Ecol Sociobiol* **47**, 400–412.
- Simmonds, E. J., Armstrong, F., and Copland, P. J. (1996). “Species identification using wideband backscatter with neural network and discriminant analysis”, *ICES J Mar Sci* **53**, 189–195.
- Simmons, J. and Chen, L. (1989). “The acoustic basis for target discrimination by FM echolocating bats”, *J Acoust Soc Am* **86**, 1333–1350.

- Simmons, J. and Vernon, J. (1971). “Echolocation: Discrimination of targets by the bat, *Eptesicus fuscus*”, *J Exp Zool* **176**, 315–328.
- Stanton, T. K. (1988). “Sound scattering by cylinders of finite length .1. fluid cylinders”, *J Acoust Soc Am* **83**, 55–63.
- Stanton, T. K. and Chu, D. (2000). “Review and recommendations for the modelling of acoustic scattering by fluid-like elongated zooplankton: euphausiids and copepods”, *ICES J Mar Sci* **57**, 793–807.
- Stanton, T. K., Chu, D., and Wiebe, P. H. (1998a). “Sound scattering by several zooplankton groups. II. scattering models”, *J Acoust Soc Am* **103**, 236–253.
- Stanton, T. K., Chu, D., Wiebe, P. H., and Clay, C. S. (1993). “Average echoes from randomly oriented random-length finite cylinders: Zooplankton models”, *J Acoust Soc Am* **94**, 3463–3472.
- Stanton, T. K., Chu, D., Wiebe, P. H., Martin, L. V., and Eastwood, R. L. (1998b). “Sound scattering by several zooplankton groups. I. Experimental determination of dominant scattering mechanisms”, *J Acoust Soc Am* **103**, 225–235.
- Stanton, T. K., Wiebe, P. H., Chu, D., Benfield, M. C., Scanlon, L., Martin, L., and Eastwood, R. L. (1994). “On acoustic estimates of zooplankton biomass”, *ICES J Mar Sci* **51**, 505–512.
- Starr, R. and Thorne, R. (1998). “Acoustic assessment of squid stocks”, in *Squid recruitment dynamics. The genus *Illex* as a model. The commercial *Illex* species. Influences on variability.*, edited by E. O. R. Rodhouse, P.G.; Dawe, FAO Fisheries Technical Paper, 376 edition (FAO, Rome).
- Urlick, R. J. (1983). *Principles of Underwater Sound*, 3rd edition (McGraw-Hill, New York).
- Vel'min, V. A. and Dubrovskiy, N. A. (1976). “On the analysis of pulsed sounds by dolphins [in Russian]”, *Proceedings of the Academy of Sciences of USSR* **225**, 470–473.

- von Helversen, D. (2004). “Object classification by echolocation in nectar feeding bats: size-independent generalization of shape”, *J Comp Physiol A Sens Neural Behav Physiol* **190**, 515–521.
- von Helversen, D. and von Helversen, O. (2003). “Object recognition by echolocation: A nectar-feeding bat exploiting the flowers of a rain forest vine”, *J Comp Physiol A Sens Neural Behav Physiol* **189**, 327–336.
- Wiebe, P. H., Stanton, T. K., Benfield, M. C., Mountain, D. G., and Greene, C. H. (1997). “High-frequency acoustic volume backscattering in the Georges bank coastal region and its interpretation using scattering models”, *IEEE J. Ocean . Eng.* **22**, 445–464.
- Williams, L. W. (1909). *The Anatomy of the Common Squid, Loligo pealii, Lesueur* (Library and Printing-Office late E.J. Brill, Leiden-Holland,).
- Yeh, C. (1967). “Scattering of acoustic waves by a penetrable prolate spheroid. I. Liquid prolate spheroid”, *J Acoust Soc Am* **42**, 518–521.
- Zakharia, M. E., Magand, F., Hetroit, F., and Diner, N. (1996). “Wideband sounder for fish species identification at sea”, *ICES J Mar Sci* **53**, 203–208.
- Zimmer, W. M. X., Johnson, M. P., Madsen, P. T., and Tyack, P. L. (2005). “Echolocation clicks of free-ranging Cuvier’s beaked whales (*Ziphius cavirostris*)”, *J Acoust Soc Am* **117**, 3919–3927.